Optical Materials: X 24 (2024) 100371

Contents lists available at ScienceDirect

Optical Materials: X

journal homepage: www.journals.elsevier.com/optical-materials-x

Invited Article

Unusually high oxidation states of manganese in high optical basicity silicate glasses

Amir Ashjari [a], Brian Topper [a,b,c], Lars H. Hess [d], Lucas Greiner [a,e], Jared Tolliver [b], Fiona Cormack [a], Dimitrios Palles [f], Efstratios I. Kamitsos [f], Mikhail G. Brik [g,h,i,j,k], Doris Möncke [a,*]

[a] Inamori School of Engineering at the New York State College of Ceramics, Alfred University, Alfred, NY, 14802, USA
[b] Center for High Technology Materials, University of New Mexico, Albuquerque, NM, 87106, USA
[c] Department of Materials Science and Engineering, Clemson University, Clemson, SC, 29634, USA
[d] Northvolt AB, Ackumulatorvägen 1, Västerås, Sweden
[e] Department of Material Science and Engineering, Missouri University of Science and Technology, Rolla, MO, 65409, USA
[f] Theoretical and Physical Chemistry Institute, National Hellenic Research Foundation, Athens, Greece
[g] School of Optoelectronic Engineering & CQUPT-BUL Innovation Institute, Chongqing University of Posts and Telecommunications, Chongqing, 400065, People's Republic of China
[h] Centre of Excellence for Photoconversion, Vinča Institute of Nuclear Sciences - National Institute of the Republic of Serbia, University of Belgrade, Belgrade, Serbia
[i] Faculty of Science and Technology, Jan Długosz University, 42200, Częstochowa, Poland
[j] Institute of Physics, University of Tartu, W. Ostwald Str. 1, Tartu, 50411, Estonia
[k] Academy of Romanian Scientists, Ilfov Str. No. 3, Bucharest, Romania

ARTICLE INFO

Keywords:
Cesium-barium metasilicate
High optical basicity
Resonance Raman enhancement
Mn^{5+}
Mn^{6+}
Redox equilibria
Optical spectroscopy

ABSTRACT

Unusually high oxidation states of manganese were stabilized within a cesium-barium silicate (CBS) glass system of extremely high optical basicity. The highest basicity was obtained for the metasilicate glass $40Cs_2O$–$10BaO$–$50SiO_2$ (mol%) with an optical basicity of $\Lambda = 0.81$. The presence of Mn^{5+} (d^2) as well as Mn^{6+} (d^1) is confirmed by UV–Vis, photoluminescence, and Raman spectroscopy. The UV–Vis spectrum is dominated by the Mn^{3+} (d^4) absorption at 526 nm for low-basicity glasses, which is replaced by a peak at 679 nm (Mn^{5+}) and, finally, a band at 603 nm (Mn^{6+}) in the glass with the highest basicity ($\Lambda = 0.81$). In this glass, the Mn^{5+}/Mn^{6+} ratio varies with the melting conditions. Photoluminescence (PL) spectroscopy under 633 nm excitation confirms the presence of Mn^{5+}, showing the narrow, forbidden $^1E \rightarrow {}^3A_2$ transition located at 1191 nm with vibrational sidebands at 1245 nm and 1290 nm. The measured static fluorescence intensity due to Mn^{5+} grows exponentially with increasing optical basicity. The near infrared fluorescence decay was bi-exponential, with time constants of 14 and 51 μs. The absence of Mn^{4+} in CBS glasses was confirmed by PL and electron paramagnetic resonance (EPR) spectroscopy. Despite initial doping as MnO_2, metastable Mn^{4+} disproportionates into lower and higher valent manganese species, followed by reduction or oxidation of manganese to a stable species as ruled by the basicity of the glass and oxygen availability during melting. A structural study of the glasses by Raman spectroscopy revealed a resonance enhancement effect for the symmetric stretching mode of MnO_4-tetrahedra at ~800 cm^{-1} with overtones observed at higher frequencies.

1. Introduction

Compared to inorganic complexes, polyvalent ions in glasses show a smaller range of oxidation states [1–7]. Some elements, especially those with less than half-filled valence orbitals can be stabilized in several valences. Examples span from Cr^{2+} (d^4) to Cr^{6+} (d^0), or from V^{2+} (d^3) to V^{5+} (d^0) [8–11]. For 3d transition metal elements, with more than half-filled valence orbitals, such as manganese, divalent and trivalent ions are acknowledged in glasses. Some elements, such as the structural probe ions nickel and cobalt are generally considered to be only present in glasses as divalent ions - where the change in coordination from tetrahedral in high-basicity glasses to octahedral in low-basicity glasses

* Corresponding author.
E-mail address: moncke@alfred.edu (D. Möncke).

https://doi.org/10.1016/j.omx.2024.100371
Received 20 June 2024; Received in revised form 5 September 2024; Accepted 1 October 2024
Available online 5 October 2024

is discussed in the literature, together with possibly other transitional states [2–4,12–16]. While high valence manganese species (Mn^{4+}, Mn^{5+}, Mn^{6+}, Mn^{7+}) are well known for manganese complexes in solution, crystalline materials, and some glass-ceramics [17–27], the rare reports for the glassy state seem to arise from misassignments of actual Mn^{2+} luminescence to Mn^{4+}, the valence inferred from the raw material used. The high stability of Mn^{2+} and Mn^{3+} when doping with MnO_2 is for example discussed by Capobianco et al. or Zandoná et al. [28,29].

The reported crystals or glass-ceramics containing higher oxidation state Mn species are all of high optical basicity, referring here to the acid/base concept established by Duffy and Ingram [30–33], see also Refs [1,2] for details on calculations applied in this study. In high-basicity glasses, dopants such as transition metal ions are found in similar chemical surroundings as in highly-concentrated basic solutions, leading to comparable spectroscopic results [1,30,33–35]. Optical basicity compares the electron donor power of the glass matrix to that of CaO, which by definition has an optical basicity $\Lambda(CaO) = 1$. While the optical basicity derives from the constituents' polarizabilities, Duffy and other researchers also showed that a higher optical basicity Λ correlates linearly with the oxygen fugacity and thus, with the ability to stabilize higher oxidation states of polyvalent ions [35–38]. It should be noted, however, that diverse oxidation states in glasses can be attained not only by selecting different glass compositions but also indirectly through modifications of the melting conditions. For instance, variations in the melting temperatures, melting times, and cooling rates can result in glasses containing high-temperature or non-equilibrium states [10,11,35,37,39,40]. Additionally, adjustments to the melting atmosphere can lead to variations in oxygen fugacity, thereby influencing the oxidation states [2,35,36,38,41].

Despite the commonly accepted restriction of certain oxidation states in common glasses, Dietzel and Coenen successfully stabilized trivalent Co^{3+} in high alkali silicate glasses in 1961 [42]. The formation of Co^{3+} - as well as Ni^{3+}- was corroborated in 2002 by one of the authors of the current manuscript, when theoretical deliberations for a maximized theoretical optical basicity led to a cesium-barium metasilicate glass [15]. This same cesium-barium silicate glass system was used a dozen years later in a bachelor thesis, where Lars Hess successfully stabilized Mn^{5+} and Fe^{4+} [43]. The high hygroscopicity of this glass, paired with high chemical activity and some unexpected findings, e.g. resonance Raman effect, required additional work and delayed the publication of these findings.

Before focusing on the specifics of this current study, it should be noted that revisiting manganese-doped CBS glasses was also sparked by the advancement of applications that exploit photoluminescence properties of active materials with highly oxidized Mn ions [17,44–46]. For example, publications on the photoluminescing properties of materials doped with Mn^{4+}, which displays a red emission after excitation by a blue light-emitting diode (LED) attracted attention [47,48]. On the other hand, even higher oxidized Mn^{5+} displays in crystalline materials a relatively narrowband emission peaking between 1150 and 1200 nm, and being characterized by long lifetimes of hundreds of microseconds [20]. Various phosphate, vanadate, and silicate crystals with Mn^{5+} received attention in the 1990s as potential laser materials [19,49,50]. Recently, a small surge in work focusing on spontaneous emission of Mn^{5+} has occurred seeking to leverage the behavior for imaging, phosphors, and thermometry [17,46,51–53]. These studies prompt the question if it is possible to prepare bulk glasses that contain significant amounts of Mn^{5+} as potential vitreous candidates for such applications. Even though we know *a priori* that the glasses of the current study are hygroscopic and are intrinsically limited for applications as they are; this work demonstrates the ability of oxide glasses to accommodate pentavalent manganese without significant contributions of lower valent manganese species – while being prepared in larger amounts than allowed by levitation melting as employed by Zandoná et al. [28,41]. Furthermore, our high-basicity glasses stabilized even hexavalent Mn^{6+}, which to our knowledge has not yet been reported in the glass literature. Moreover, this current study provides a very detailed spectroscopic description, allowing for subsequent studies on chemically more stable compositions.

As indicated above, the current glass system was selected for its high optical basicity rather than its chemical stability. Glasses in series (100-x-y)SiO_2–xCs_2O–yBaO (with x = 25 to 40, y = 10–14 mol%) were additively doped with 0.05–0.5 mol% of manganese dioxide (MnO_2). The valence and coordination of the dopant in the obtained glasses were inferred from spectroscopic data employing UV–Vis, photoluminescence, Raman, and EPR spectroscopies. Inorganic reference materials $K_2[Mn(IO_3)_6]$, and aqueous solutions of K_3MnO_4, K_2MnO_4, and $KMnO_4$, were synthesized as spectroscopic standards for Mn^{IV}, Mn^{V}, Mn^{VI}, and Mn^{VII}, respectively. Raman spectroscopy was used to determine the glass structure and to provide additional evidence for Mn^{5+} and Mn^{6+} through strong resonance Raman enhancement phenomena of MnO_4^{3-} and MnO_4^{2-}, respectively

Since the selection of a glass system with extremely high optical basicity was crucial in the successful preparation of highly oxidized 3*d* ions, the concept of optical basicity and how it was applied in the current study will be reviewed briefly in the following section, followed by a succinct summary of ligand field theory as applied to manganese, before discussing sample preparation and our spectroscopic measurements by UV–Vis, photoluminescence, EPR and Raman spectroscopy.

1.1. Optical basicity theory

Optical basicity allows us to classify different oxide glasses within the well-known spectroscopic series, and also to deduce the expected oxidation state of manganese polyvalent ion [30,32,35,54]. Duffy and Ingram [31,32,54] explained in their concept of optical basicity how the glass matrix affects the oxidation states of metal ions in vitreous systems, based on acid-base behavior, which is affected by the electronegativity (Pauling scale) and the size of the binding orbitals (orbital overlap). Thus, Duffy and Ingram argued that the electron density of oxygen is very high in SiO_2, while it is in a "floppy" state when oxygen atoms are loosely bonded to modifier cations such as K^+, or even more so in $Cs^+ \cdots$ O–Si bonds. Systems with a high concentration of "floppy" bound oxygen atoms are better able to stabilize high valence dopants and ions in low coordination numbers than can tightly bound electrons in low-basicity glasses. Thus, high levels of low-field strength modifier oxides in alkali-alkaline earth-silicate glasses can be expected to shift the redox equilibrium of polyvalent ions to higher oxidation states [34,35].

Optical basicity *(Λ)*, provides a measure of the electron donor power of the glass matrix and is given in dimensionless numerical values. Λ was originally derived from the optical spectroscopic peak shift measurement for a probe ion, e.g. Pb^{2+} added in mere traces to the glass sample, relative to the band maximum observed for the same probe ion in CaO. The latter is used as the standard and has been set as $\Lambda(CaO) = 1$. The optical basicity of a glass (macro or average basicity) depends on the basicity values of each individual oxide component (cation oxide basicity Λ_i). The macro basicity is additively derived from the optical basicity values of each constituent elemental oxide, by considering the oxygen equivalent fraction (X_i), which should not be confused with the molar fraction of $(M^{n+})_2O_n$ since X_i considers the number of oxygen atoms *n* of each element oxide,

$$\Lambda_{macro} = \sum X_i \bullet \Lambda_i \qquad \text{Eq. (1)}$$

Cation oxide basicity values, Λ_i, have been determined for most element oxides and the compiled values can be found in the literature [1,31,32], the most complete and relatively recent list was compiled by Rodriguez et al. [55]. It should be noted that the concept of optical basicity can equally be applied to non-oxide glasses [56–58]. In the current study, we use $\Lambda(SiO_2) = 0.48$, $\Lambda(BaO) = 1.33$, and $\Lambda(Cs_2O) = 1.52$ [55,59]. Variations can be found for average optical basicity, that is, calculated values or those determined through an empirical

correlation to the oxygen polarizability as determined from refractive index and density measurements, and those basicities determined via probe ions, where the latter often selectively seek out sites of higher basicity [32,34,60,61]. Even though micro-basicities can change in sites with a higher or lower number of non-bridging oxygen atoms, or even with a change of coordination, the attractiveness of the concept of optical basicity is that the macro-basicity values of glasses can be calculated for any glass composition regardless of prior knowledge of the glass structure.

1.2. Ligand field theory and spectroscopy

Ligand field theory allows us to deduce the different electronic configurations of a d-metal ion complex from optical spectra, including the ion's valence, coordination, and even variations in the bonding type (degree of covalence - ionicity) [3–7]. Standard methods for the determination of a complex's symmetry, the ion's energy levels, and the ligand field splitting energy are UV–Vis and photoluminescence spectroscopy. Electronic transitions, which are measured by UV–Vis-spectroscopy, are either prohibited intrinsic excitations from a d-metal orbital to another d orbital in the same ion or quantum mechanically allowed charge-transfer (CT) transitions from the ligand to the metal and vice versa abbreviated as "LMCT" and "MLCT", respectively [1,4,7,62]. CT bands often have high energies and are found in glasses below or near the intrinsic cut-off wavelength [62].

On the other hand, Laporte or parity-forbidden excitations of *d-d* valence electrons are theoretically described by discrete energy levels for which a change in the orbital quantum number $\Delta l = 0$ applies [3,7,63]. Such transitions between states of the same parity of the same ion are forbidden and have a significantly lower intensity than the excitation of charge-transfer bands in which the orbital quantum number changes. For the Laporte rule to be applied in its "ideal form", the dopant complex should have a center of inversion – otherwise, the odd and even states (parity of states) cannot be distinguished. Since a non-distorted octahedron exhibits such a center of inversion, and a tetrahedron does not, the selection rules are relaxed, and the *d-d* transitions of tetrahedra are "less forbidden" (i.e. have higher oscillator strengths). However, even in octahedral coordination, such transitions can still be observed, and as distortions lead to stronger deviations from ideal symmetry, the *d-d* transitions' intensities are enhanced, as seen for example by the relatively strong coloring effect of Jahn-Teller distorted Cu^{2+} ions [1,3,4,6,12,64] or the strong colorant Mn^{3+} ions discussed in this study. Additionally, another rule called the "spin or multiplicity rule" states that the total spin multiplicity must remain unchanged throughout a transition. In a d^5-high spin complex, in which all levels are occupied by spin-rectified electrons, an excitation leads to spin pairing, and thus, the change in total spin multiplicity cannot be avoided. Transitions that require a change in the electron spin have a very low probability and are subsequently of very low intensities, as can be seen by the faint orange Mn^{2+} d^5 ion, which is often described as colorless when not present in very high concentrations [3,4,6,57]. It should be noted that spin-orbit interaction can mix up the states with different multiplicities, leading to so-called "intensity borrowing". In this process, wave functions, like those of spin doublet states, incorporate some elements from the spin-quartet states, and vice versa. As a result, this leads to the slight lifting the spin-selection rule [65].

For ions with several possible electronic transitions, having numerous valence electrons and "holes", where "holes" denote empty orbitals which can be occupied by the excited electrons, multiple electronic transitions occur between the states determined by the Russel-Saunders coupling and crystal field splitting. The exact allocation of the bands might be complicated by additional band splitting due to Jahn-Teller distortion, vibronic progressions, and possible coexistence of different emitting centers. For energetically degenerate states, complexes can remove the state degeneracy by distortions of their initially highly symmetrical structure. The removal of degeneracy causes some terms to experience a significant energy reduction. As a result, the total energy of the complex decreases, but the stability increases. From the electronic transitions, the energy levels and the ligand field stabilization or ligand field stabilization energy (Dq or Δ_0) and the Racah parameter (B) can be obtained. To calculate these parameters, only the absorption levels and the complex's symmetry are required, as the energies of the various absorption band maxima are projected onto the Tanabe Sugano diagrams [45,48,63,64,66,67].

1.3. Manganese in glasses and complexes and respective spectroscopic evidence

Many *d-d* transitions fall in the visible wavelength range and give rise to often vivid colors [2–4,6,7,45]. In glasses, manganese ions are usually found either in the divalent or in the trivalent state. Mn^{2+} ions are often referred to as colorless, but in high concentrations, they impart a weak orange color to glasses [61,68]. Mn^{3+} ions are strong colorants, and low dopant concentrations result in deep purple glasses [2–4,12,28,61,69]. Contrary to crystals, where Mn^{4+} has been identified in some compounds [44,68], to the best of our knowledge, there are no convincing reports on Mn^{4+} in glasses. Most often, an actual Mn^{2+} fluorescence is mistaken for Mn^{4+}, and the more convincing reports concern Mn^{4+} within crystals that are embedded within the glass, rather than Mn^{4+} ions dissolved within the vitreous matrix [26]. The most intense of the double forbidden transition of Mn^{2+} is from the $^6A_{1g}(^6S)$ ground state to the $^4A_{1g}(^4D)$ or the $^4E_g(^4D)$ excited states, absorbing near 420 nm (23800 cm^{-1}) [34,61,69]. Mn^{3+} on the other hand, features a strong Laporte forbidden but spin-allowed transition from the $^5E_g(^5D)$ ground state to the $^5T_{2g}(^5D)$ excited state at around 500 nm (20000 cm^{-1}). This transition gives rise to the intense purple color which is typical for Mn-doped glasses and, even traces of Mn^{3+} often conceal the weak absorption of Mn^{2+} [69]. Tetravalent manganese has been added to glasses since ancient times as a decolorant and MnO_2 has been dubbed glass makers soap for its oxidizing properties [3,29]. MnO_2 is metastable and easily reduces in soda lime silicate glasses to Mn^{3+} or even Mn^{2+}, oxidizing the strongly colored blue divalent iron ions (d^6) to the weak yellow, since spin-forbidden, trivalent Fe^{3+} (d^5). Irradiation of manganese-doped glasses often results in the photo-oxidation of Mn^{2+} to $(Mn^{2+})^+$ hole center, and recoloring of glasses initially having been decolored by MnO_2 addition [3,7,65,70,71].

Electron Paramagnetic Resonance (EPR) spectroscopy can selectively probe the paramagnetic ions Mn^{2+} and Mn^{4+}, providing information on bonding sites and coordination symmetry [61,68,79]. Mn^{3+} however gives no EPR signal, being a Kramer ion, and EPR signals for Mn^{5+} and Mn^{6+} have been reported for low temperatures and/or Q band frequency only. Thus, even though Mn^{2+} is hardly active in the optical spectra, it can easily be identified by its very intense and characteristic EPR signals, even when only present at trace levels [4,61]. This can be illustrated by Mn-free fluoride phosphate glasses made from ultra-pure optical-grade raw materials with iron levels below 10 ppm, which nevertheless show the Mn^{2+}-sextett in their EPR spectra [85].

2. Experimental section

2.1. Glass preparation

Three glass compositions were prepared to achieve different, though generally high optical basicity samples, with Λ ranging from $\Lambda = 0.715$ to $\Lambda = 0.814$. Glass names (Table 2) end on the first two decimals of the glass basicity. Glass batches for 10–30 g of glass were placed in Al_2O_3 or platinum crucibles and melted in a muffle furnace, at melting temperatures of 1100–1450 °C for 15–240 min. Melting conditions had to be varied slightly for different glass compositions but were also altered to investigate the effect of melting conditions on the oxidation state of manganese. Undoped base glasses, as well as glasses doped with 0.05–0.5 mol% MnO_2 were prepared. Systematic changes in the melting

Table 1
Overview of spectroscopic parameters of various Mn^{n+} species in solution, glasses, or crystalline materials, including estimates for the molar absorption coefficient ε at the respective band maxima.

Optical Parameter	Mn^{2+} (d^5)	Mn^{3+} (d^4)	Mn^{4+} (d^3)	Mn^{5+} (d^2)	Mn^{6+}(d^1)
Absorption Maxima (nm)	420 [61,68]	480-520 [69,72]	330, 465 [73]	670-680 [17,28]	570-610 [74]
ε ($Lmol^{-1}cm^{-1}$)	0.1–0.5 [69,72]	~104[a], 25–135 [72,75]	Not available	~275[a]	~800[a]
PL (ex/em) (nm)	ex: ~420 em: 500–530 (T_d green) and 600–680 (O_h red) [61]	ex: 480-520 em: 700 (Max), also 850 and 1100 [76]	ex: 460-470 em: 670–720 [73, 77]	ex: 630-680 em: 1120–1200 (T_d, CN = 4) [17,20,20,23,53]	Ex: 550–580 Em: 900–1200 [25,27,78]
EPR Signal	Sextet, g~2, g~3.3, & g~4.3 [61,79,80]	EPR inactive (Kramer ion) [81]	Singlet, g~2 [82]	EPR at broadband and low temperatures [78, 83]	EPR at broadband and low temperatures [84]
CT Band (nm)	230 [62]	380-390 [62]	290-300 [73]	320-350 [17,46,53]	280-290 and 400–460 [22,25,74]

[a] Values are calculated from spectra of CBS81 glasses doped with 0.05 mol% MnO_2 (see Fig. 2), using samples with thickness $d = 1.25$ (Mn^V) and $d = 1.45$ (Mn^{VI}), large error margin of ± 50 % should be considered for the calculated value due to the uncertainty of the species' concentrations (actual redox ratios), variations in sample thickness, and possible evaporation as the main error sources. The value $\varepsilon_{510} \approx 104\ Lmol^{-1}cm^{-1}$ results when assuming only Mn^{3+} to be present in CBS72.

Table 2
Nominal glass compositions and dopant levels in mol%, and selected properties such as optical basicity *delete* (Λ) and color, using basicity values Λ(Cs_2O) = 1.52, Λ(BaO_2) = 1.33, and Λ(SiO_2) = 0.48 from Ref. [55].

Name	SiO_2	Cs_2O	BaO	Dopant (MnO_2)	Λ	Color
Mn-CBS72	61	25	14	0.05–0.5	0.715	purple
Mn-CBS76	56	32.5	11.5	0.05–0.5	0.759	bluish purple
Mn-CBS81	50	40	10	0.05–0.5	0.814	green/blue/ turquoise

conditions and crucible materials did result in systematic changes in the hues of Mn-doped glasses, each connected to significant spectral changes. Apparently, as will be discussed in this work, in glasses with high optical basicity the Mn^{5+}/Mn^{6+} ratio is sensitive to doping level, melting time, melting temperature, surface area of the melt, and crucible type. Melts are reproducible as long as comparable melting parameters are chosen. Due to their high basicity and low SiO_2 content, the glasses are highly hygroscopic. This leads to immediate uptake of atmospheric humidity, which, depending on the season and ambient humidity, can cause complete dissolution of the splat-quenched glass shards within a couple of hours. Therefore, the glasses were usually splat quenched between brass blocks and immediately measured or transferred into desiccators and stored under dry argon or nitrogen atmosphere in sealed tubes. Preheating the brass block to 450 °C minimizes thermal stress and larger samples of even thickness could be obtained for optical measurements. Preheating would not change the observed color of the samples in any significant way. Likewise, for external measurements, individual fragments of the quenched samples were placed directly into polymer cuvettes for photoluminescence measurements, or into quartz tubes for EPR measurement, and in either case, purged with dry N_2 or Argon before sealing for transport and measurements.

The density of three of each undoped CBS72, CBS76, and CBS81 samples was ~3.920, 4.105, and 4.232 g/cm^3 on average. Each measurement was repeated 5 times, using the Archimedes method in ethanol, on a Mettler Toledo, ME104/00 density measurement setup, yielding a± 0.005 g/cm^3 reproducibility. The density values of the CBS81 samples doped with 0.05 mol% of MnO_2 melted in Pt crucible for 20 and 180 min, as well as the samples melted in alumina crucibles for 20 and 150 min were measured separately for two samples of each. The density of 0.05Mn-CBS81 melted in Pt for 20 min is 4.232 g/cm^3 (average of 5 measurements) which decreases to 4.094 g/cm^3 by increasing melting time to 180 min. The density of 0.05Mn-CBS81 melted in alumina for 20 min is 4.216 g/cm^3 (average of 5 measurements) which decreases to 4.035 g/cm^3 when increasing the melting time to 150 min. The 4.232 and 4.035 g/cm^3 densities were used for the calculation of the reported extinction coefficient values of Mn^{5+} and Mn^{6+} in Table 1 for the corresponding samples, respectively (see also Fig. 4, for the corresponding UV–Vis spectra of the samples).

2.2. Reference materials preparation

2.2.1. Mn^{6+}: MnO_4^{2-} aqueous solution

A thick dark green MnO_4^{2-} solution was prepared following the procedure of Ref. [86], by pouring 12 g of $KMnO_4$ into 60 ml of concentrated KOH solution (12 M). The reaction mixture was heated under reflux for 2 h. Initially, a dark brown color due to $MnO(OH)_2$ was observed, which turned into a murky green after some time. Finally, as the reaction was completed, the reaction mixture turned to a crystal clear dark green. The resultant mixture was cooled to 3 °C and any $MnO(OH)_2$ precipitate which formed during cooling was filtrated. The final solution was stored under an argon atmosphere in the dark at 3 °C to prevent any subsequent redox processes. The material was diluted with 12 M KOH before measuring by UV–Vis spectroscopy using PMMA

cuvettes.

2.2.2. Mn^{5+}: MnO_4^{3-} solution

The MnO_4^{3-} solution was prepared from the previous MnO_4^{2-} solution by reduction with a deactivated reducing agent (Na_2SO_3). 20 ml of the MnO_4^{2-} solution were cooled to −15 °C and diluted with 80 ml of 12 M KOH under vigorous stirring. Sodium sulfite was slowly added to the mixture with a molar excess of 1.2 (relative to MnO_4^{2-}). The solution turned to deep blue and the optical spectra were measured without delay since autocatalytic degradation induced by MnO_2 starts immediately [87]. The samples were diluted with 12 M KOH before measuring by UV–Vis spectroscopy using PMMA cuvettes.

2.2.3. Mn^{4+}: $K_2[Mn(IO_3)_6]$ powder

Highly reactive manganese was required for the reaction and, therefore, 1.4 g of $MnSO_4$ was poured into a solution of 40 ml 12 M KOH while dripping slowly 7 ml of 33 % H_2O_2 into the mixture which was heated to 100 °C. The mixture turned into a flaky brown solid of $MnO(OH)_2$, which was cooled to room temperature and afterward filtrated. The solid obtained was washed with distilled water. Wet reactive $MnO(OH)_2$ was used directly in the preparation of $K_2[Mn(IO_3)_6]$ using the method of Berg [88]. For this, 1 g of wet $MnO(OH)_2$ was added to a mixture of 50 ml water, 8 g HIO_3 (excess), and 15 g KIO_3 (excess). The mixture was boiled for 1 h until a yellow solid materialized out of the brownish solution. The slurry was then boiled under vigorous stirring for another hour until it turned into an intense brown color. The solid was filtered, washed with distilled water, and then dried. $K_2[Mn(IO_3)_6]$ is not easily dissolvable and therefore no optical spectra were obtained; however, this material was used as a reference for Mn^{4+} in EPR spectroscopy.

2.3. Spectroscopy

Initial UV–Vis–NIR spectra of splat quenched samples were collected using a double-beam spectrophotometer (Cary 5000, Agilent Technologies) in the range of 200–1600 nm with a resolution of 2 nm. In summer, the spectrometer was purged with dry air to prevent the dissolution of the hygroscopic samples in the warm, humid air. Additional transmission spectra were taken later on a PerkinElmer Lambda 950, over the range of 200–1500 nm with 1 nm resolution.

Fluorescence measurements were conducted at room temperature on glasses packaged under inert gas flow inside clear cuvettes. A 633 nm helium-neon laser was used as the excitation source. A 100 mm focal length lens focused the beam onto the specimen inside the cuvette. A 105 μm core diameter step index multimode fiber placed near the outer cuvette wall collected the fluorescence and served as the input to a Yokogawa AQ6370D optical spectrum analyzer. Spectra were collected over the range of 1000–1500 nm with a 2 nm resolution averaging 12 acquisitions per point. Considering the mobility of the samples in the cuvette, careful action was taken to ensure the separate measurements were nominally identical by keeping the beam path and collection fiber location fixed while maximizing the fluorescence signal through the cuvette position.

Fluorescence lifetime measurements were made using a 40 mW 633 nm diode laser as an excitation source directly modulated to create square pulses approximately 10 μs wide with <2 μs fall time. The optical pulse was monitored with a Si detector to trigger fluorescence measurements. The beam was focused onto the glass contained inside a cuvette. The fluorescence was subsequently collected with a lens array and passed through a 1000 nm long pass filter. An InGaAs detector with 1 MHz bandwidth acquired the near-infrared fluorescence and was recorded in averaging mode on an oscilloscope.

EPR spectra were recorded using the X-Band frequency of a Bruker system equipped with internal spin and g-value calibration. The samples were placed into high-purity SiO_2-tubes of 10 mm diameter directly after glass preparation. The tubes were filled with argon to prevent hydrolyzation of the samples until and during EPR measurements.

Raman spectra were measured in the backscattering configuration on a WITec Alpha300 using various laser excitation lines. The 355 nm laser used a 20×, and the 488 nm and 633 nm lasers had a 50× objective.

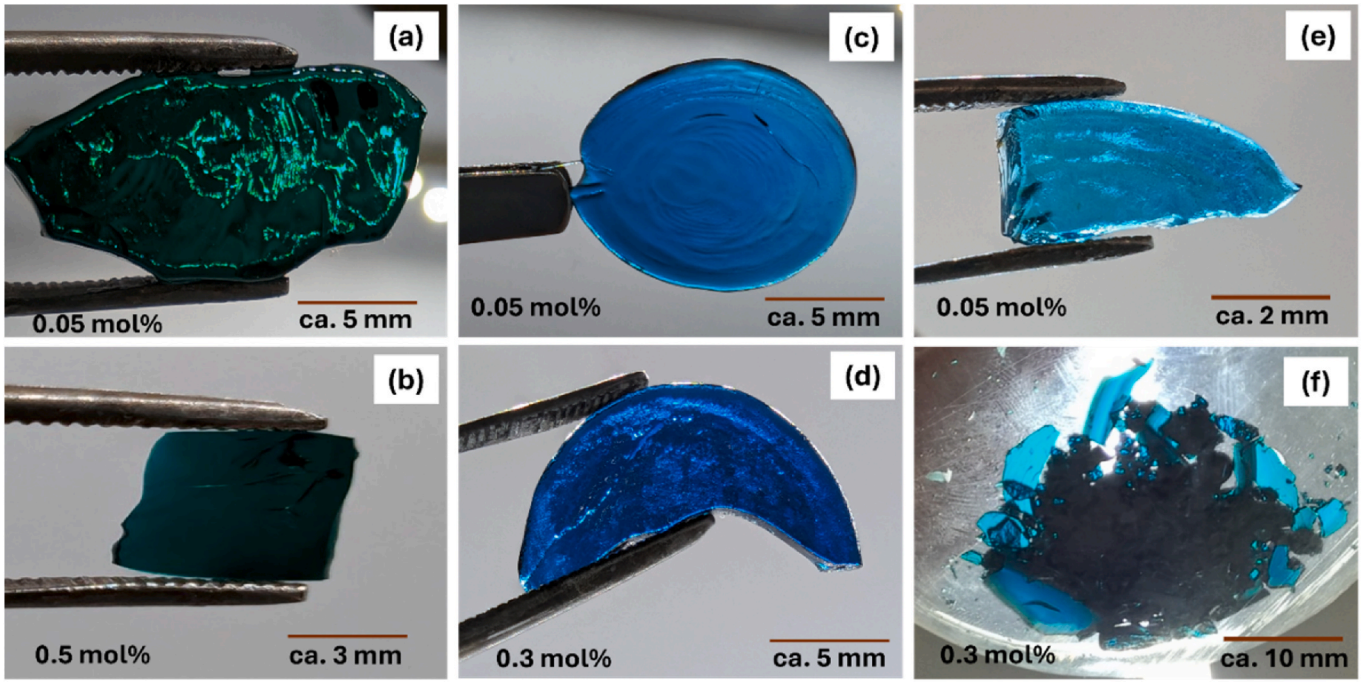

Fig. 1. Photographs of splat-quenched CBS81 glass, showing various colors depending on the MnO_2 doping levels (indicated in mol% in the images), melting conditions, and sample thickness (d in mm). (a) and (b) melted in Pt crucible at 1250 °C for 20 min, with (a) $d = 1.25$ and (b) 0.5–1.5 mm; (c) and (d) melted in Pt crucible at 1300 °C for 180 min, with (c) $d = 1.45$ and (d) 1.15 mm; (e) and (f) melted in alumina crucible at 1300 °C for 150 min, with $d = 1.40$ mm (e), while the thicknesses vary from 0.5 to several mm for the samples stored in a silica flask under the inert argon atmosphere (f). (For interpretation of the references to color in this figure legend, the reader is referred to the Web version of this article.)

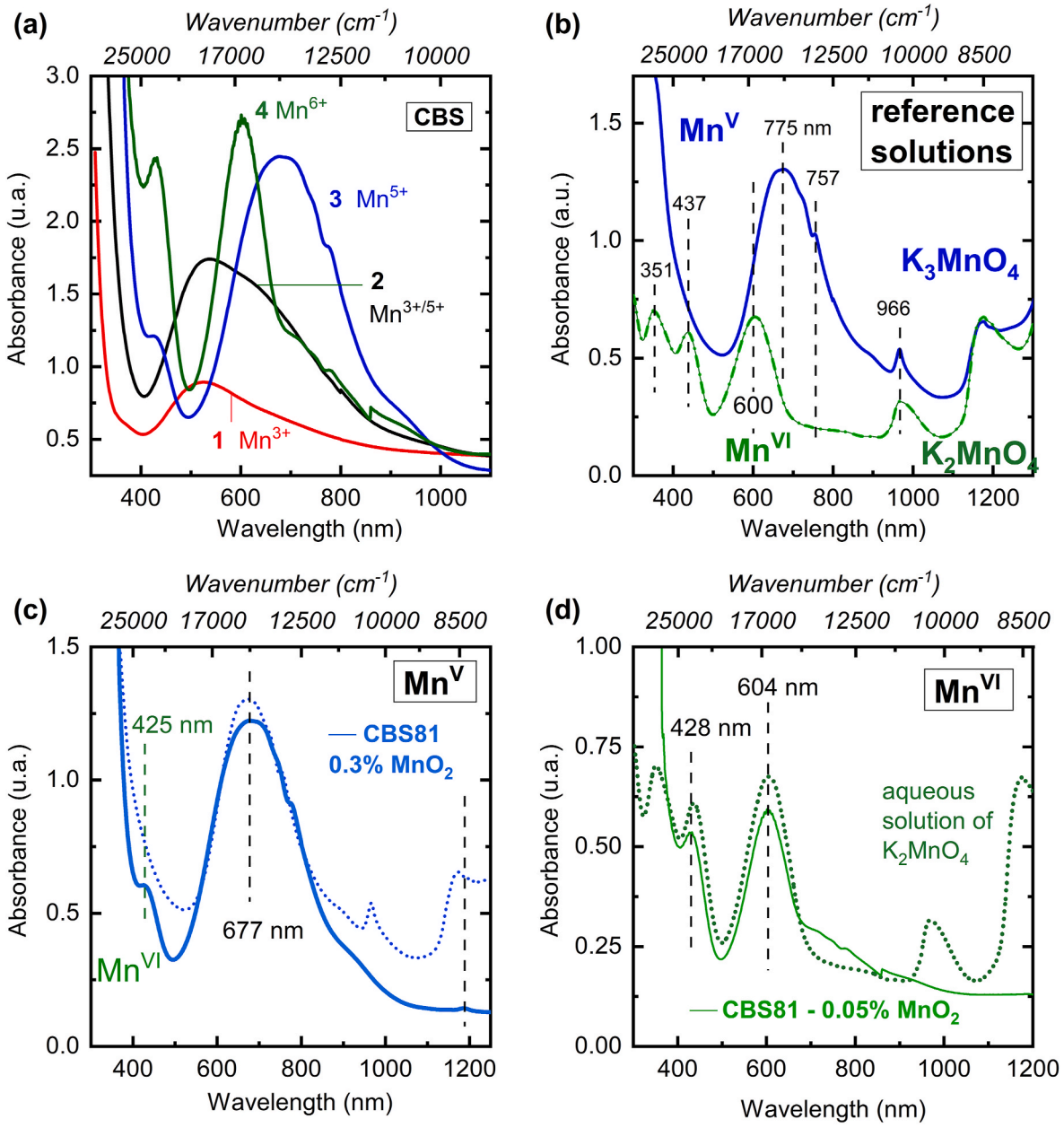

Fig. 2. (a) UV–Vis spectra of four Mn doped CBS glasses, including three glasses of different optical basicity with nominal 0.3 mol% MnO_2: (1) CBS72, almost pure Mn^{3+}, red line; (2) CBS76 glass with evidence for both Mn^{3+} and Mn^{5+}, black line, (3) CBS81, represents predominantly Mn^{5+}, blue line and (4) CBS81 with only 0.05 mol% MnO_2, mostly as Mn^{6+}. (b) UV–Vis spectra of aqueous solutions of the reference materials: (1) 12 M KOH solution with K_3MnO_4 for Mn^{5+}, blue line, and (2) 12 M KOH solution of K_2MnO_4 for Mn^{6+}, green line. (c) Direct comparison of the Mn^{5+} spectra of 0.5Mn-CBS81 (a3) with the reference (b1); and (d) direct comparison of the Mn^{6+} spectra of 0.05Mn-CBS81 (a4) with the reference (b2) (spectra in c and d are normalized for comparable intensities, glass thickness d ranges from 0.2 to 3 mm). (For interpretation of the references to color in this figure legend, the reader is referred to the Web version of this article.)

Spectra were averaging 20 accumulations using 20 s integration times. The samples were measured with all three lasers at exactly the same spot. Repeat measurements at other spots, this time in a different order of excitation wavelengths, confirmed that no laser damage nor any significant water uptake occurred.

3. Results and discussion

3.1. Optical spectroscopy I: UV–Vis absorption

Fig. 1 shows images of six metasilicate CBS81 glass samples prepared at varying melting conditions containing either low MnO_2 levels of 0.05 mol% (top row) or higher doping levels of 0.3–0.5 mol% (lower row).

The optical spectra of all the glasses from Fig. 1 are shown in Figs. 2–4 and will be discussed in detail in the following section. Fig. 1a and b shows the green-hued CBS81 samples that contain mostly Mn^{6+}, after melting in a Pt crucible at 1250 °*C* for 20 min, doped with 0.05 (1a) or 0.3 mol% MnO_2 (1b). The blue glasses (containing mostly Mn^{5+}) shown in Fig. 1c, d are melted in Pt crucibles at 1300 °*C* for 180 min, and the glasses were also doped respectively with 0.05 and 0.3 mol% MnO_2. Finally, samples melted in alumina crucible at 1300 °*C* for 150 min are presented in Fig. 1e, f showing the bright turquoise color of a mixture of Mn^{5+} and Mn^{6+}, also having Mn^{5+} as the majority species. It is worth noting that the samples with 0.05 mol% MnO_2 are significantly more transparent than those with higher concentrations (0.3 and 0.5 mol%). However, for instance, the samples melted in alumina crucibles (Fig. 1e

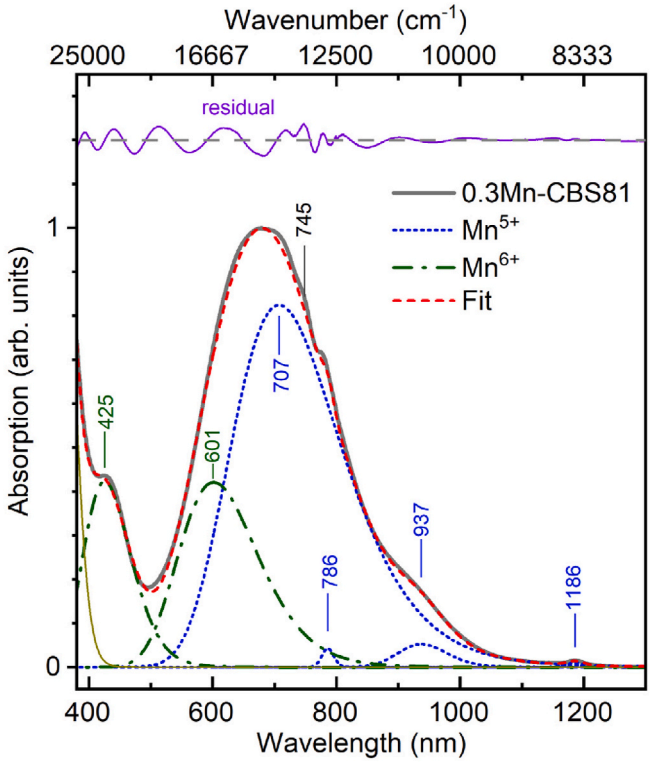

Fig. 3. Decomposition of the 0.3Mn-CBS81 absorption spectrum into Gaussian components corresponding to tetrahedral Mn^{5+} and Mn^{6+} electronic transitions (here, the wavenumber fit is replotted over wavelength for better comparison with Fig. 2, see also Fig. S1 in the SI for the original fit using wavenumbers regime). The thin solid green line below 400 nm has been added to account for the absorption cut-off, most likely due to a charge transfer band, and thus account for a background correction. (For interpretation of the references to color in this figure legend, the reader is referred to the Web version of this article.)

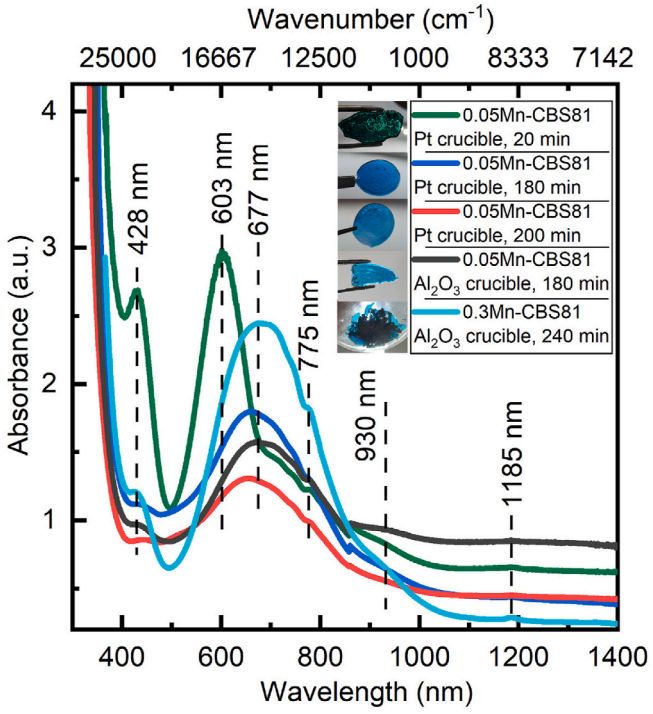

Fig. 4. UV–Vis Spectra of CBS81 samples doped with MnO_2, melted under different melting conditions resulting in a variable distribution of Mn^{5+} and Mn^{6+} species, leading to glasses from dark green (mostly Mn^{6+}) to bright cyan/turquoise (mostly Mn^{5+}). Spectra are not normalized to sample thickness; samples were not polished prior to measurements. (For interpretation of the references to color in this figure legend, the reader is referred to the Web version of this article.)

and f) have a very similar appearance and color in the images, mainly because the glass shards with 0.3 mol% MnO_2 are much thinner compared to the sample with 0.05 mol%. These higher-doped glasses had been prepared first, and most spectroscopic studies (photoluminescence, electron paramagnetic resonance, and Raman) were conducted on these glasses, and therefore these glasses will be discussed in more details in sections 3.2 to 3.4, respectively.

Fig. 2a depicts the optical spectra of four cesium-barium silicate glasses of three different silicate contents, which will be discussed in the following in order of increasing optical basicity. The first glass CBS72 (1) is of purple color and displays the typical broad absorption band of Mn^{3+}, which extends from 400 to 800 nm and has an absorption maximum at 526 nm (19010 cm^{-1}). The CBS76 glass (2) also displays the band of Mn^{3+}, with the same maximum absorption at 526 nm. However, a shoulder around 680 nm indicates the emergence of another Mn-species and the color changes to a bluish purple. The glass of the highest basicity, Mn-CBS81, is bright turquoise (Fig. 1f), and has its absorption maximum at 679 nm (14730 cm^{-1}), as seen in spectrum 3 of Fig. 2a. Spectrum number 4 corresponds to the green glass in Fig. 1a and was a later melt of CBS81 with very low MnO_2 levels of only 0.05 mol%. After comparison of the glass spectra with those of reference materials containing different confirmed Mn species (see Fig. 2b) the additional absorbing species can be identified as Mn^{5+} and Mn^{6+}. The observed absorption envelops agree also with other crystalline Mn^{5+}-containing materials or solutions reported in the literature [17,26,28,89]. The broad band of spectrum (3), 0.3Mn-CBS81, reaching from 500 to 1000 nm with the max at 680nm and two pronounced shoulders at 775 and 930 nm is the characteristic absorption band of Mn^{5+} in tetrahedral symmetry. These absorption bands are assigned to spin-allowed $^3A_2$ (^3F) → $^3T_1$ (^3F), spin forbidden $^3A_2$ (^3F) → $^1A_1$ (^1G), and spin allowed $^3A_2$ (^3F) → $^3T_2$ (^3F) transitions, respectively. Finally, another band around 1187 nm is observed in the high-basicity glass 0.3Mn-CBS81, in agreement with that reported for crystalline materials [17,19] and this was attributed to the spin forbidden $^3A_2$ (^3F) → $^1E_1$ (^1D) transition of Mn^{5+}, resulting in a low-intensity band.

Fig. 2c shows the direct comparison of the spectrum (3) of Fig. 2a with the reference spectrum of dissolved pentavalent Mn^V. The 0.3Mn-CBS81 glass also displays a distinct band around 420–430 nm, visible as a shoulder in the UV/Vis cut-off, which is located near 425 nm (23255 cm^{-1}) in all green and turquoise glasses (see spectrum (4) in Fig. 2a and 2d). In the reference solution of Mn^{6+} the ca. 425 nm band can be assigned to a charge transfer transition of oxygen to hexavalent manganese [25,78].

The main band envelop of the d^1 ion Mn^{6+}, (4) in Fig. 2a, is peaking at 603 nm (16580 cm^{-1}), reaching from ca. 500–680 nm, and is much narrower than the d-d transitions of Mn^{5+}. The visible spectrum of the 0.05Mn-CBS81 glass, the main band at 603 nm, and the shoulder at 425 nm align almost seamlessly with the reference spectrum of dissolved K_2MnO_4 containing hexavalent Mn^{VI} only (see Fig. 2d). The glass contains a low intensity, broad shoulder at 700 nm, indicating the presence of some Mn^{5+} ions, which are absent in the reference solution.

To investigate the ligand field and Racah parameters, the absorption spectrum of Mn-CBS81 was fit with Gaussian bands in the frequency (i.e., wavenumber) space (Fig. 3, see also SI for the original data (Fig. S1) and ref [90] for information on the band decomposition process). The CBS glass in Fig. 2d has well-resolved Mn^{6+} bands at approximately 23530 (425 nm) and 16630 (601 nm) cm^{-1} arising from LMCT and ^2E → $^2T_1$ transitions. These band positions are not assumed to change in the CBS glass of Fig. 2c where Mn^{5+} dominates, but the presence of Mn^{6+} is clearly contributing to the overall absorption profile. According to the fitting results, the ground state absorptions for Mn^{5+} from $^3A_2$ to ^1E,

$^3T_2(^3F)$, $^1A_1$, and $^3T_1(^3F)$ are centered at 8428, 10670, 12726, and 14140 cm^{-1}. Using the $^3A_2 \rightarrow {}^3T_1(^3F)$ transition from the fitted band at 14140 cm^{-1}, ligand field, and Racah parameters Dq, B, and C values of 1067 cm^{-1}, 329 cm^{-1}, and 2928 cm^{-1}, respectively, are obtained. Alternatively, using 14706 cm^{-1} (680 nm), where the measured absorption peak for $^3A_2 \rightarrow {}^3T_1(^3F)$ is found, gives Dq, B, and C values of 1067 cm^{-1}, 397 cm^{-1}, and 2669 cm^{-1}, correspondingly. The values for Dq and B are smaller than in crystalline yttrium orthosilicate [91] ($\Lambda(Y_2SiO_5) = 0.79$), which appears to be the only silicate documented containing tetrahedrally coordinated Mn^{5+}. In Y_2SiO_5 the ligand field splitting energy and Racah values are Dq = 1133 cm^{-1}, B = 550 cm^{-1}, and C = 2255 cm^{-1}.

Yttrium aluminum perovskite, $\Lambda(YAlO_3) = 0.805$, can host stable mixed Mn^{4+}/Mn^{5+} concentrations [92]. As will be discussed later, Mn^{4+} does appear weakly in the EPR signal of the CBS glasses of the current study, and this alternative assignment for the wide, low-intensity component band at 13420 cm^{-1} (745 nm), constituting a shoulder in the spectrum of Fig. 3, should not be ignored. This band could be due to $^4A_2 \rightarrow {}^2E$ absorption of Mn^{4+} [92]. From this perspective, the broad absorption band at 23529 cm^{-1} (425 nm) in the CBS glasses could also be receiving contributions from Mn^{4+}: $^4A_2 \rightarrow {}^4T_2$ [44,67]. However, in light of the shown stabilization of Mn^{6+} as the majority species in some of our CBS glasses, the 425 nm band is most likely a charge transfer transition of Mn^{6+} [25,78].

The reference material for Mn^{4+}, $K_2[Mn(IO_3)_6]$ powder, cannot be easily dissolved or diluted for optical transmission spectroscopy. While no optical spectrum of Mn^{4+} was obtained, powdered material could be used for EPR studies, see **Section 3.3**. Considering the absence of additional bands in the glassy samples, in agreement with literature reports that MnO_2 is a metastable state [3,29], it is assumed that if any manganese is oxidized to the tetravalent state, Mn^{4+} will initially disproportionate into an equal amount of lower and higher valent manganese ions, e.g. Mn^{3+} and Mn^{5+}, before, depending on optical basicity and oxygen fugacity, the respective stable oxidation state will form, the melt taking up oxygen from the atmosphere for oxidation or releasing molecular O_2 when being reduced [28,35,41].

The UV–Vis spectra of five CBS81 glasses doped with 0.05 and 0.3 mol% of manganese, melted under different conditions, are shown in Fig. 4. The data indicate that lower melting times and low temperatures, as well as the use of platinum crucibles, favor the stabilization of Mn^{6+} as the majority species in the glasses. In contrast, higher melting temperatures, longer holding times, or the use of alumina crucibles support the stabilization of Mn^{5+} as the predominant species. It was assumed that higher melting temperatures and longer melting durations might lead to higher cesium evaporation and/or dissolution of the alumina crucible into the glass. These processes both lower the optical basicity for the final glass, and thus favor Mn^{5+} over Mn^{6+}. As was mentioned earlier in the experimental section (**section 2.1**), the density measurements showed a noticeable drop, ~0.2 g/cm^3 (~5 %), in the density of the glass by increasing the melting time from 20 min to 150 or 180 min. With Λ (Cs_2O) = 1.52, any cesium loss will significantly lower the optical basicity. ICP-OES measurements confirmed a decrease in Cs concentration of ~10 % (see also Fig. S2a in the SI). Additionally, the temperature itself may affect the redox equilibrium [35].

3.2. Optical spectroscopy II: photoluminescence emission

The photoluminescence spectra of the three glasses with varying basicity, but all doped with 0.5 mol% MnO_2, taken under 633 nm excitation, are presented in Fig. 5a. It is evident from Fig. 2c, that 633 coincides with an absorption band of Mn^{5+}, the excitation spectrum of Mn^{5+} (see SI, Fig. S3, taken later with a different setup confirms that the employed laser matches the excitation maximum very well). The basic spectrum that is seen for all glasses, is dominated by the main emission due to the $^1E_1$ (^1D) → $^3A_2$ (^3F) transition of Mn^{5+}. The main peak position due to the pure electronic transition lies at 1191 nm, commensurate with Mn^{5+} in other oxide materials [17,18,46]. The FWHM of the 1191 nm peak is approximately 30 nm, which is, as expected for a glass, broad compared to the same emission in crystalline hosts. The vibrational sidebands are seen in the measured spectra as features with maxima at approximately 1238 and 1300 nm, corresponding to the ν_2 (319 cm^{-1}) and ν_1 (704 cm^{-1}) vibration modes of the MnO_4^{3-} anion (see Raman section 3.4.2). This fluorescence is observed in all samples (left inset), and its integrated intensity appears to grow exponentially with

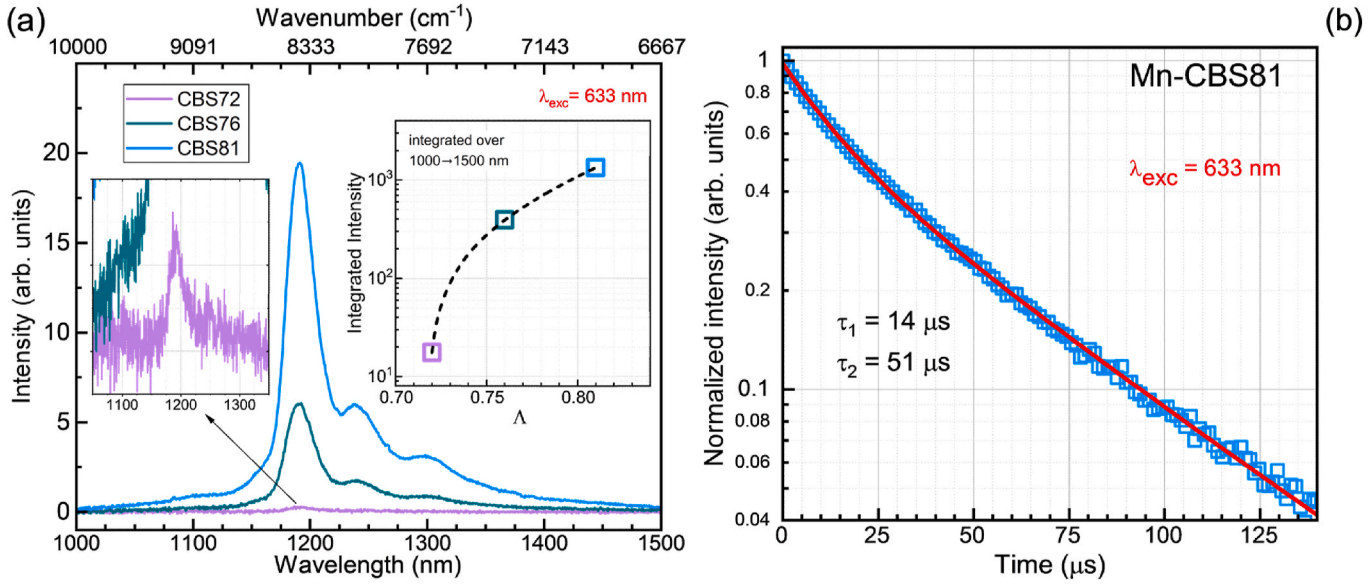

Fig. 5. (a) NIR photoluminescence spectra of Mn-CBS glasses containing 0.5 mol% MnO_2. The excitation source was a 633 nm laser. The inset on the left is a magnification of the central line, demonstrating that a trace of Mn^{5+} is present even in CBS72. The right inset shows how the integrated photoluminescence intensity of the Mn^{5+} increases with the optical basicity value of the glasses, where the dashed line is a fitted exponential growth function to guide the eye. (b) Broadband detection (1000–1500 nm) of the near-infrared photoluminescence decay of Mn^{5+} in Mn-CBS81 glass, measured after 633 nm excitation (see also SI, Fig. S3, for the full excitation spectrum Mn^{5+} in CBS glass). The open blue squares are experimentally measured, and the solid red line is a bi-exponential fit. (For interpretation of the references to color in this figure legend, the reader is referred to the Web version of this article.)

increasing optical basicity of the glass (right inset). The broad Mn^{6+} fluorescence at 900–1200 nm in the near-infrared, as described in the literature [25,27,78], might be contributing to the weak broad emission shoulder in these CBS samples (more observable in CBS81, see also the excitation/emission spectrum presented in Fig. S3) under 633 nm excitation.

The fluorescence decay of Mn^{5+} in Mn-CBS81 glass after pulsed 633 nm excitation is shown in Fig. 5b. The decay is bi-exponential (solid line fit) with a fast decay of 14 μs and a long decay of 51 μs. The bi-exponential behavior could be due to concentration quenching as seen in Mn^{2+}-containing glasses [93]. Quenching from hydroxyl species cannot be excluded. Another plausible explanation is that the fast component is due to the quenching of Mn^{5+} sites by Mn^{6+} sites, for which the near-infrared decay is typically much faster than that of Mn^{5+}. More comprehensive investigation would be required to elucidate the influence of various factors on the lifetime of Mn^{5+} in high-basicity glasses. In any case, it is worth noting that the long lifetime component measured here of 51 μs is close to the 69.5 μs lifetime of Mn^{5+} in Y_2SiO_5 at room temperature [94].

The typical Mn^{2+} related fluorescence with broad emission maxima between 450 nm and 600 nm, shifting from green in tetrahedral coordination to orange in octahedral coordination [61], could not be detected in Mn-containing CBS81 glasses after excitation near 410 nm using a commercial fluorescence spectrometer. As mentioned in the introduction, reports of Mn^{4+} in glasses were often mistakenly associated with the broad emission band of Mn^{2+}. Certified Mn^{4+} bearing crystals are characterized by a sharp emission peak at 625 nm, though the position of the excitation band depends strongly on the composition, for example at 360 and 460 nm for Na_2SiF_6 and at 340 and 418 nm for K_2SiF_6 [44]. A broader emission band at 686 nm was reported α-ZnP_2O_7 after excitation at 230 nm [68]. While none of these excitations resulted in measurable emissions in the CBS glasses, it should be noted that, if these emission processes were taking place, significant reabsorption by Mn^{5+} may preclude their observation.

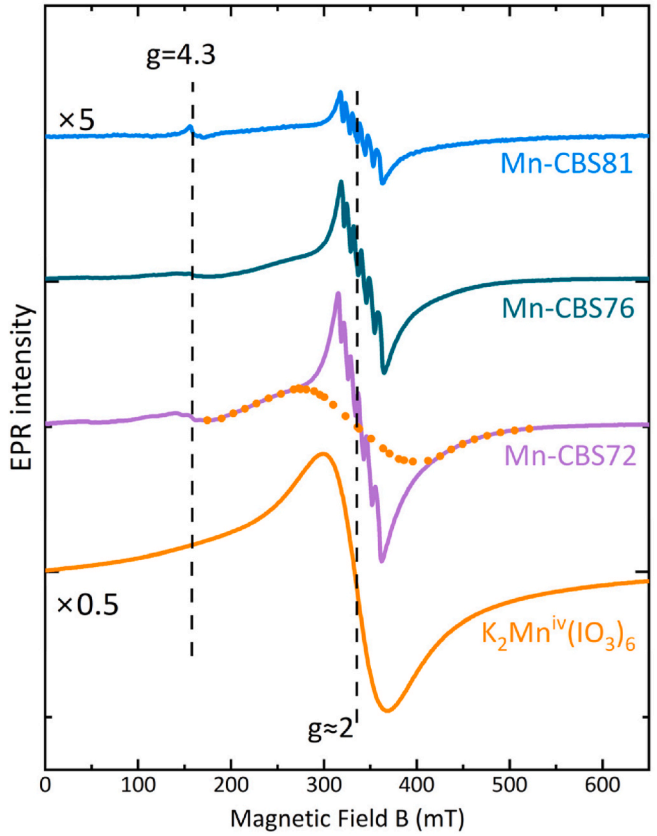

Fig. 6. EPR spectra of the Mn-containing CBS glasses and of the tetravalent Mn^{4+}-containing reference material $K_2[Mn(IO_3)_6]$. The top spectrum was magnified by a factor of 5, the bottom spectrum was reduced by a factor of 2. The broken line in the spectrum of the glass CBS72 indicates the contribution of the broad singlet of Mn^{4+}.

Optical spectroscopy shows that Mn^{3+} is prevalent in the CBS glass of the lowest basicity and the amount of Mn^{5+} increases with increasing optical basicity of the samples, which is further supported by the increasing photoluminescence intensity. Fluorescence spectroscopy throughout this investigation provided no evidence for the presence of lower valent Mn^{4+} and Mn^{2+} in any significant amount - both of which would show very different emission and excitation bands than Mn^{5+} [47,61,93].

3.3. Electron paramagnetic resonance (EPR) spectroscopy

EPR-spectroscopy is a very sensitive and often selective method for the qualitative and quantitative analysis of paramagnetic ions [4,95]. EPR active manganese species are Mn^{2+} and Mn^{4+}, while Mn^{3+} and Mn^{5+} are silent Kramer ions not known to give any specific signals in glasses when measured at room temperatures [73,78]. Fig. 6 shows the EPR spectra of Mn-containing glasses and the reference material $K_2[Mn(IO_3)_6]$ containing tetravalent Mn^{4+}. Even in low concentrations, paramagnetic Mn^{2+} ions give a characteristic sextet signal [14,61,79,82,95]. The tetravalent Mn^{4+} ion on the other hand, only shows a broad singlet EPR signal [20,82,96]. Both, the main EPR resonance of Mn^{2+} and Mn^{4+} ions are centered at g-values of g~2 [20,61,79,82]. The smaller resonance at g = 4.3 is typical for d^5 ions Mn^{2+} and Fe^{3+} in less symmetric, more distorted sites [61,79,95].

The sextet of divalent manganese is clearly apparent in all three glasses, even in the one of the highest basicity. However, it should be noted that in Fig. 6, the spectrum of sample CBS81 with the highest basicity needed to be amplified by a factor of 5 for reasonable detail, indicating that Mn^{2+} is only present in traces. Mn^{2+} is one of the most sensitive ions for EPR measurements in glasses and even when using high purity raw materials, the sextet is often observed in non-manganese doped high purity glasses [97]. The CBS81 glass with the highest Mn^{5+} concentration clearly has the lowest concentration of Mn^{2+}, and also the lowest intensity for the underlying singlet signal of Mn^{4+}. Careful inspection of all glass spectra shows a broad Mn^{4+} singlet superimposed on the Mn^{2+} sextet signal. For clarity, the singlet resonance is indicated by the broken line added to the EPR spectrum of the CBS72 glass.

Since the sample geometry and volume of the glasses was not identical, as quenched samples were transferred into quartz tubes after melting, we did not attempt any further quantification of the different paramagnetic Mn species. Overall, both EPR-active species occur as minority species of the various redox equilibria, they favor the higher oxidized manganese species and disfavor the reduced Mn^{2+} as well as the thermodynamically meta-stable Mn^{4+}. This notion is supported by the fact that both paramagnetic species are detectable in similar proportions in all the Mn-doped glasses, even in the glass with the most oxidized Mn species. If an increase in the optical basicity would simply shift progressively the fraction of all manganese species in favor of the higher oxidation states, $Mn^{2+} \rightleftharpoons Mn^{3+} \rightleftharpoons Mn^{4+} \rightleftharpoons Mn^{5+} \rightleftharpoons Mn^{6+}$, we would expect to observe a shift in the relative EPR intensities from Mn^{2+} to Mn^{4+} in glass matrices with higher oxidation potential, that is from CBS72 to CBS81, as shown in Fig. 6.

All optical and EPR measurements confirm that the thermodynamically unfavorable MnO_2 used for batching, disproportionates initially during melting into Mn^{3+} and Mn^{5+}, and the available oxygen at the melt's surface in conjunction with the optical basicity of the glass will either reduce Mn^{5+} to Mn^{3+} (CBS72) or oxidize most of the Mn^{3+} to Mn^{5+} (CBS81) or even Mn^{6+} [28,35,41]. Other than in glasses, thermodynamical adversity can be overcome in certain complexes and glass ceramics [44,47,82].

3.4. Raman spectroscopy

3.4.1. Raman spectra of undoped glasses

Raman spectroscopy of undoped glasses was initially utilized to obtain information on the silicate glass structure of these highly modified glasses, including the available ligand sites or water content. Fig. 7a compares the cesium-barium metasilicate composition CBS81 of this study to sodium and potassium metasilicates reported by Brawer and White [98], and Fig. 7b presents the Raman spectra of the three undoped CBS72, CBS76, and CBS81 glasses obtained using a 488 nm excitation laser source. This comparison is primarily useful because the Raman lineshape character and band frequencies change with modifier cation mass in some oxide systems [99]. Since the silicate network structure is secondary in this study and a significant compositional gradient is not employed, this notion enables an insightful approximation as to the silicate speciation in these CBS glasses. In alkali silicates, narrower lineshapes have been documented for heavier alkali modifiers, attributed to decreasing disorders i.e., lower variation in bond length/angles of the network forming species, and less disproportionation between silicate species [100,101]. Downshifts of vibrational bands with heavier charge balancing cations are documented in some oxide crystals and glasses, although the driving mechanism remains subject to debate and might be connected to the number of ionic bonds formed between non-bridging oxygen atoms and various modifier cations [102].

The Raman spectra of Na and K metasilicate glasses were observed to be very similar to their crystalline analogues, which are comprised of infinite chains of Q^2 silicate tetrahedra with two bridging and two non-bridging oxygen atoms. The dominating high frequency peak between 950 and 985 cm^{-1} is due to the stretching of $Si–O^-$ bonds, $\nu(Si–O^-)$, in Q^2 species, where Q^n denotes a silicate tetrahedron with n bridging oxygen atoms. In particular, the Q^2 species are present in metasilicate chain-like arrangements and the $\nu(Si–O^-)$ band downshifts with increasing mean modifier cation size. Relative to the crystalline analogues, the features to higher and lower frequencies have greater relative intensity in glasses, likely due to silicate tetrahedra with higher and lower charge environments than the metasilicate, i.e., resulting from disproportionation of $2Q^2 \leftrightarrows Q^1 + Q^3$. A feature most likely belonging to $\nu(Si–O^-)$ in Q^1 species downshifts from 855 cm^{-1} (Na) to 830 cm^{-1} (K) and to 821 cm^{-1} (Cs/Ba). The middle frequency region has a band between 560 and 615 cm^{-1} due to the symmetric stretching/bending vibration of metasilicate Si–*O*–Si bridges, with likely some contribution from network deformations involving Q^3 species. A shoulder around ~700 cm^{-1} in the Na and K glass becomes a distinct feature in the Cs/Ba-metasilicate glass and this can be attributed to pyrosilicate bridges in $Si_2O_7^{6-}$ [103,104]. The apparent decoupling of this mode in the Cs/Ba glass could be due to decreased disorder, including reduced disproportionation in the heavy modified glass [100], narrowing the bandwidth of all meta- and pyro-bridge modes, or perhaps related to differences in the lengths of chain-like structural units arising from cation-size induced effects. However, it is important to keep in mind that the spectra for the K and Na metasilicate glasses are taken from the literature and were not measured on the same instrument as the Cs/Ba glass of the current study. At lower frequencies, a band of medium intensity appears at ca. 300 cm^{-1} in the spectra for glasses with heavier cations than Na, and this might be due to the bending of silicate tetrahedra with non-bridging oxygen atoms.

With this structural picture of the cesium-barium metasilicate glass in mind, the other Cs/Ba silicates in Fig. 7b can be discussed. With increasing silica content, the relative intensity of the low-frequency range appears to decrease as the number of non-bridging oxygen decreases. The band at ~600 cm^{-1} becomes more intense indicating a larger number of Si–*O*–Si bridges as the SiO_2 content increases and, therefore, increased network connectivity. The pyrosilicate bridge activity at ~700 cm^{-1} is clearly observed for CBS81, but as the SiO_2 levels is higher in CBS76 and CBS72, this signature is nearly absent. Furthermore, increased silicon dioxide content leads to the presence of more Q^3 species, and the high-frequency region is now dominated by the peak at 1078 cm^{-1} in CBS72. This is in line with the decreasing O to Si ratio.

Despite the high hygroscopicity of the CBS glasses, no significant signatures of water bands and hydrolyzation products were detected during Raman measurements. This is due to the measures taken, i.e. dry storage and climate-controlled labs which prevented significant deterioration during measurements.

3.4.2. Raman spectra of manganese-containing CBS glasses

Although the silicate glass structure is not anticipated to change with the addition of less than 1 mol percent of manganese oxide to the base glass compositions, manganese doping of 0.5 mol % resulted in an

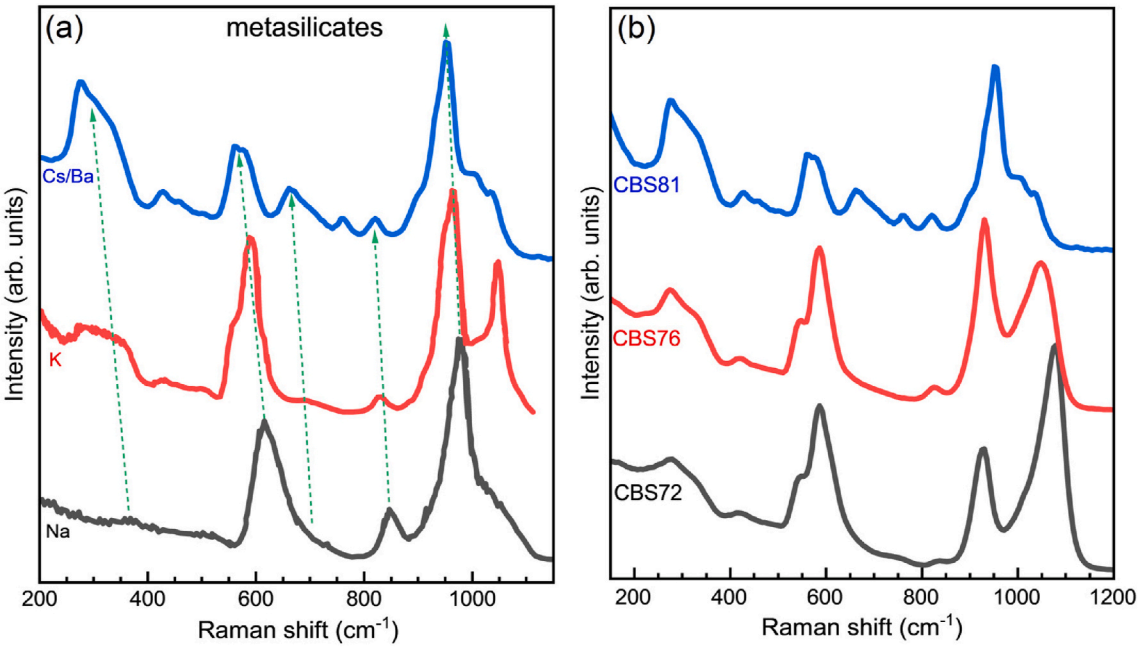

Fig. 7. Raman spectra of (a) the cesium-barium metasilicate glass CBS81 compared to two alkali (K, Na) metasilicates from Brawer and White [98], and (b) undoped CBS glasses. Raman spectra were measured with 488 nm excitation.

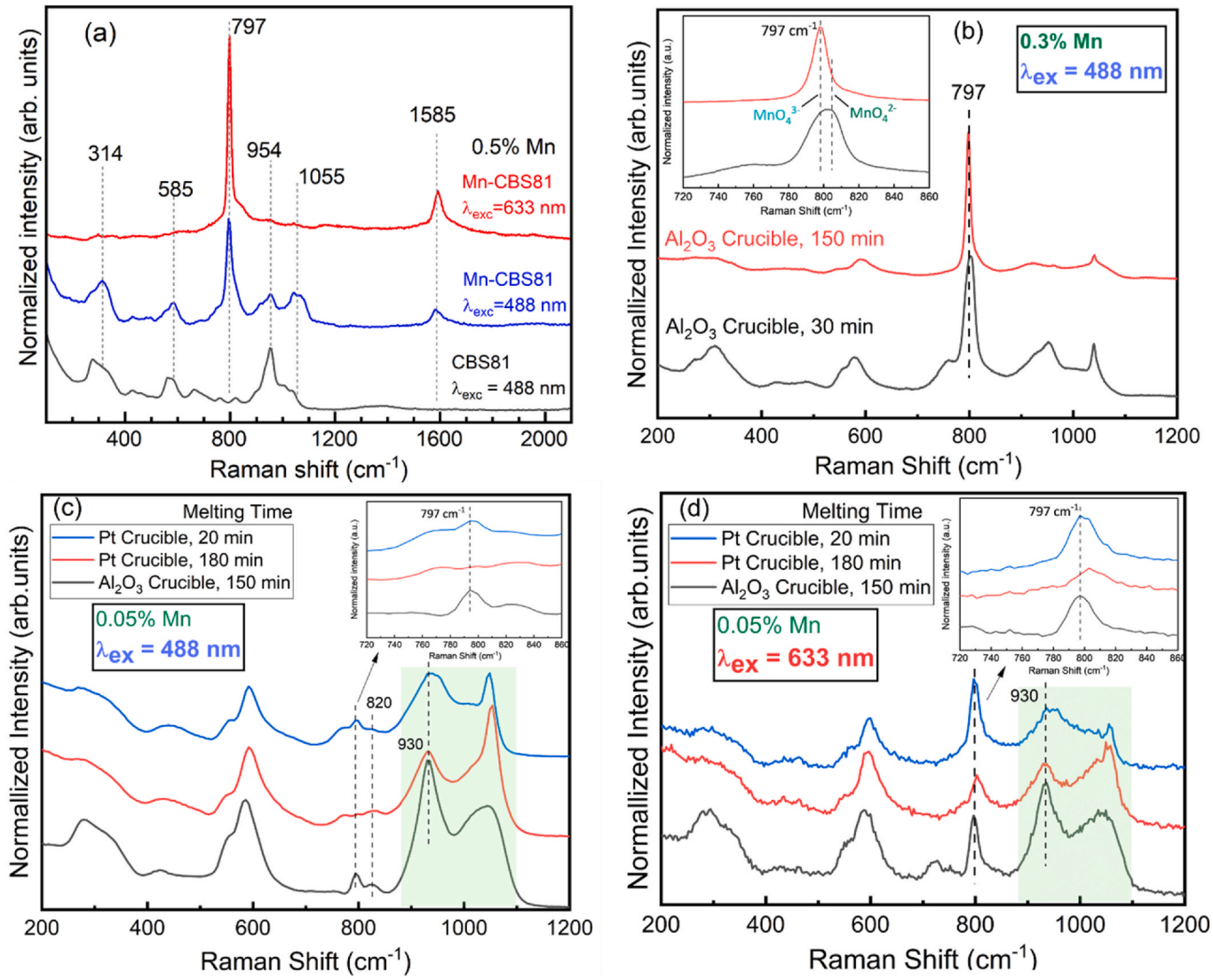

Fig. 8. (a) Raman spectra of the same spot of 0.5 mol% Mn-doped CBS81 glasses obtained with 633 nm or 488 nm excitation wavelength, compared with the undoped CBS81 taken at 488 nm excitation (the same spectrum as in Fig. 7b); (b) Raman spectra of 0.3 mol% Mn-doped CBS81 melted in alumina crucible for 30 min (dark green and more Mn^{6+}) and 150 min (more blueish turquoise color and more Mn^{5+}) with 488 nm excitation wavelength; (c) and (d) Raman spectra of 0.05 mol % Mn-doped CBS81 melted in Pt Crucible for 20 min (dark green and mostly Mn^{6+}) and 180 min (more blueish turquoise color and mostly Mn^{5+}), and the sample melted in alumina crucible for 150 min (turquoise and mostly Mn^{5+} with significant amounts of Mn^{6+}) with 488 and 633 nm excitation wavelengths, respectively. (For interpretation of the references to color in this figure legend, the reader is referred to the Web version of this article.)

intense Raman signal at 797 cm^{-1} (Fig. 8a), and even doping levels of only 0.05 mol% MnO_2 can still be detected by this signal. However, the intensity of this signal depends strongly on the chosen laser excitation wavelength, the band being enhanced by excitation at 633 nm relative to 488 nm. The enhancement of Raman scattering of certain modes is due to excitation at a wavelength that overlaps with an electronic transition of the scattering species, and this is known as the resonance Raman effect. The effect was for example reported in detail for TiO_4 groups in silica glass (ULE) by Efthimiopoulos et al. [105].

Inspection of Fig. 8a shows immediately the sharp feature at 797 cm^{-1} in the Mn-doped CBS81 spectra. This band is assigned to the symmetric stretching mode (ν_1) of the MnO_4^{3-} anion [106]. The scattering intensity at 797 cm^{-1} is greater for 633 nm excitation, due to the enhancement achieved by increasing overlap with the absorption band at around 675 nm or 14815 cm^{-1} (Fig. 3), which is due to the $^3A_2 \rightarrow {}^3T_1(^3F)$ electronic transition of Mn^{5+}. Similar resonance Raman effects have been reported by Noda et al. [89] for Mn^{5+}-O stretching in aqueous solution of Mn^{5+}, with the intensity of the Raman signal trending with the magnitude of the absorption spectrum (actually outlining the absorption band of Mn^{6+}, under the larger Mn^{5+} absorption in their work). Overtones of the $\nu_1(Mn^{5+}$-O) feature were observed here at ~1585 cm^{-1} ($2\nu_1$) and ~2385 cm^{-1} ($3\nu_1$, not shown). Activity at 314 cm^{-1} appears strongly in the Mn-CBS81 spectra under 488 nm excitation (Fig. 8a), and is assigned to the symmetric bending mode, ν_2(O–Mn^{5+}-O) [106], consistent with the vibrational sideband of the fluorescence spectra (Fig. 4a) and previous reports [107]. The asymmetric stretching mode (ν_3) and the asymmetric bending mode (ν_4) of the MnO_4^{3-} anion are expected at ca. 785 cm^{-1} and 340 cm^{-1}, respectively, with much weaker Raman intensity than the symmetric ν_1 and ν_2 modes [106], and are not clearly visible in the measured Raman spectra.

Although the primary silicate activity at ~950 cm^{-1} is overshadowed by the strong Mn–O stretching mode at 797 cm^{-1}, the Mn-CBS81 spectrum for 488 nm excitation shows that the maximum of this band is maintained at 954 cm^{-1}. This suggests that the silicate speciation is not noticeably affected by this low Mn addition, as expected for the minimal MnO_2 concentration under consideration. Additional scatterings at 585 cm^{-1} and ~1055 cm^{-1} appear under 488 nm excitation of the Mn-CBS81 spectrum and are likely due to the combination

of low-frequency modes [46].

Mn^{5+} is typically discussed as a tetra-oxo anion or molecular ion when incorporated into inorganic crystalline materials [108,109]. Most studies appear to involve Mn^{5+} in phosphates and discuss isomorphic substitution of MnO_4^{3-} for PO_4^{3-}. The Raman spectra herein are consistent with anionic MnO_4^{3-} species stabilized inside the high optical basicity silicate glass. Strictly speaking, this should remove charged Ba^{2+} and Cs^{+} cations away from silicate species, thus repolymerizing the network to some extent. However, such an effect would be exceedingly difficult to quantify for the doping concentrations used here, without even adding to the difficulty of characterization the ephemeral nature of these glasses in laboratory conditions.

Furthermore, analyzing the spectra more accurately, an asymmetry is observable as a shoulder in the resonance ν_1 band of MnO_4^{3-} toward the higher frequencies (ca. 802 cm^{-1}) as seen in the inset of Fig. 8b. This shoulder can be related to the resonantly enhanced ν_1 mode of MnO_4^{2-} tetrahedra [106], as discussed for the UV–Vis spectra of the CBS samples that contain both Mn^{5+} and Mn^{6+} oxidation states. Therefore, we might expect to see an overlap of the ν_1 vibrational modes of MnO_4^{2-} alongside MnO_4^{3-} tetrahedra in the observed resonance band. To investigate this idea, the glasses doped with 0.3 mol% MnO_2 and melted in an alumina crucible for 30 and 150 min which show the green (more Mn^{6+}) and cyan/turquoise (mostly Mn^{5+}) features, respectively (see also the UV–Vis spectra in Fig. 4), were measured by Raman using the 488 nm excitation but selecting a grating that gives a higher resolution of 2 cm^{-1} (see Fig. 8b). Broadening of the resonance band and upshifting is observed in the sample with higher Mn^{6+} levels (the dark green samples, melted for 30 min), as shown in the inset of Fig. 8b. Interestingly, the sample with the cyan/turquoise color, containing mostly Mn^{5+}, shows a much narrower resonance band located at lower frequency (<800 cm^{-1}). This result can be attributed to the overlap of the resonantly enhanced ν_1 modes of MnO_4^{2-} and MnO_4^{3-} anions in the sample melted for 30 min, which contains similar amounts of Mn^{6+} and Mn^{5+} ions.

Fig. 8c and d shows the Raman spectra after 488 and 633 nm excitation, respectively, of 0.05 mol% Mn-doped CBS81 glass melted in Pt crucible for 20 min (dark green glass, containing mostly Mn^{6+}) and for 180 min (cyan/turquoise glass, containing mostly Mn^{5+}), and of the same sample melted in an alumina crucible for 150 min (turquoise colored glass, containing a mix of majority Mn^{5+} and some Mn^{6+}). These Raman spectra indicate that the resonance Raman effect leads to the detection of tetrahedral $Mn^{5+/6+}$-O vibrational modes even at low concentrations of only 0.05 mol%. It is apparent that samples melted in Pt crucibles for only 20 min contain mostly Mn^{6+}, while those melted in Pt crucibles for up to 200 min contain mostly Mn^{5+}. The sample melted in an alumina crucible for 150 min, contains a majority of Mn^{5+} but a slightly higher amount of the minority species Mn^{6+} than the long melts from Pt crucibles, when considering the contribution of the 428 nm band in the UV–Vis spectra in Fig. 4. The Mn–O stretching Raman signal seems overall slightly more pronounced for samples with a higher Mn^{6+} content, specifically for the spectra taken with the 488 nm laser line as this wavelength matches well with the 428 nm CT band of Mn^{6+}. This resonance Raman enhancement is higher and well pronounced even for 0.05 mol% doped samples, while not observable for the sample melted in Pt for 180 min, a sample that contains mostly Mn^{5+} (Fig. 8c). However, the later sample shows noticeable resonance enhancement when excited with the 633 nm Raman laser (Fig. 8d), but only a very weak signal is seen after using the 488 nm excitation wavelength. Not only is the 633 nm Raman laser close to the d-d band of Mn^{6+} located at ~605 nm, but also is close enough to the absorption band of Mn^{5+} at ~675 nm leading to more pronounced resonance compared to the 488 nm laser measurements. Therefore, it can be said that the resonance observed with 488 nm excitation arises mostly from MnO_4^{2-} tetrahedra of Mn^{6+} due to the 428 nm CT absorption. On the other hand, the Raman signal observed with 633 nm excitation manifests enhancement from resonance with both MnO_4^{2-} and MnO_4^{3-} species due to their d-d absorption bands at 605 and 675 nm, respectively.

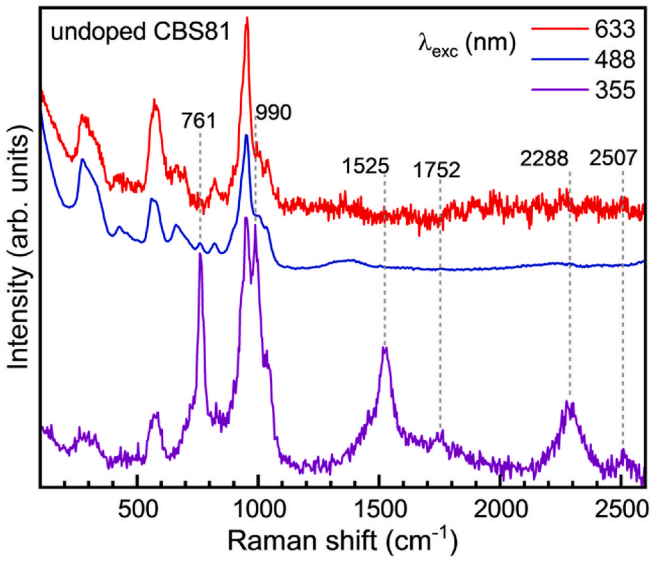

Fig. 9. Raman spectra of undoped CBS81 glass measured with excitation at 633, 488, and 355 nm.

Finally, looking at Fig. 8c and d in the Q^n bands region, 900-1100 cm^{-1}, the light green highlighted area in the figures, it is noticeable that the glass structure melted in alumina is changed compared to the glasses melted in the Pt crucible. The alumina-melted glass network seems to be more depolymerized as the band at 930 cm^{-1} has gaines relative intensity, which can be translated to creating more Q^2 units (SiO_4^{2-}). Additionally, the feature at 820 cm^{-1} has gained slightly higher intensity with both increasing melting time and melting in an alumina crucible which can be related to more Q^1 (SiO_4^{3-}) units, which means a desirable glass network/environment for the stabilization of other tetrahedra with (3-) charge, like MnO_4^{3-}. Similar structural changes have been discussed for other glasses melted in alumina crucibles, e.g. phosphates, tellurites, or silicophosphates [110].

In the discussions of Fig. 7 (Raman of the undoped glasses) and Fig. 8a (Mn resonance Raman) a feature at 761 cm^{-1} can be seen for the undoped CBS81 glass, as well as in the shoulder of the ν_1 band of MnO_4^{3-} tetrahedra in Mn-CBS81 glass under 488 nm excitation (Fig. 8a). This feature is even stronger than the 797 cm^{-1} band for Mn-doped glasses when the Raman spectra are acquired under 355 nm excitation (not shown in Fig. 8a to maintain clarity). Without the overlap of Mn related bands, the Raman spectra of undoped CBS81 glass are shown in Fig. 9 under 355, 488, and 633 nm excitation. The 761 cm^{-1} feature is intense and sharp under 355 nm excitation, weak for 488 nm excitation, and undetectable amidst the noise in the 633 nm excitation spectrum. The intensity dependence on excitation wavelength along with the narrow lineshape is indicative of an additional resonance Raman enhancement via a UV transition, probably a CT transition. The 761 cm^{-1} feature has overtones at 1525 cm^{-1} (2ν) and 2288 cm^{-1} (3ν). It is conceivable that these bands are due to the stabilization of Fe^{4+} in the highest basicity glass due to iron oxide impurities in the raw materials [43] (the presence of iron impurity is also confirmed through ICP-OES measurements, see SI, Fig. S2b). This Raman assignment is further supported by the ν_1 mode in $Ba_2(FeO_4)$, in which the $(FeO_4)^{4-}$ anion is tabled to have ν_1 = 762 cm^{-1} dominating the Raman spectrum [108]. An additional intense feature contributes to the Si–O stretching band area at 990 cm^{-1}, along with its overtones at 1752 cm^{-1} and 2507 cm^{-1}. The origin of this activity is still under investigation, but neither of these bands was observed in lower basicity glasses. Preliminary tests on iron-doped CBS glasses (see also SI Fig. S4) show some similarities in UV–Vis spectra of the three undoped CBS glasses melted in a Pt crucible, with the spectrum of the CBS81 glass doped with 0.5 mol% Fe_2O_3 and the reference spectrum of an oxo-iron (Fe(IV)) complex. The UV–Vis absorption bands of the

undoped CBS81 glass match well with those of the reference iron(IV) complex [111], though optical bands from Pt ions would also absorb in this wavelength [112–114].

4. Conclusion

Cesium-barium-silicate glasses with high optical basicity values of 0.72, 0.76, and 0.81, labled CBS72, CBS76, and CBS81, respectively, were prepared undoped and doped with 0.05–0.5 mol% MnO_2 by melting under air followed by splat quenching. Due to the hygroscopic nature of the samples, they were immediately analyzed or stored under dry inert gas such as N_2 or Ar. According to UV–Vis spectroscopy, Mn^{5+} and Mn^{6+} were the main manganese species in the high-basicity metasilicate glass CBS81, while glass CBS76 had a mixture of Mn^{3+} and Mn^{5+}. The assignments of the high valence optical spectra were confirmed by comparison with reference materials containing Mn^{5+} and Mn^{6+} ions and reports in the literature for inorganic crystals. Mn^{5+} has a broad absorption with a maximum located at 677 nm resulting in a bright turquoise color of the samples, while Mn^{6+} gives rise to a dark green color due to the main absorption band with the maximum located at 604 nm. Stabilization of Mn^{5+} or Mn^{6+} shows a high dependence on the melting conditions, including temperature, holding time, and crucible type. The presence of Mn^{5+} in the glass was further confirmed by photoluminescence spectra of the glasses where the characteristic emission band of Mn^{5+} at 1191 nm was observed. Electron paramagnetic resonance (EPR) spectroscopy of the samples showed the absence of significant amounts of Mn^{2+} or Mn^{4+}, which are the two species of manganese that are EPR active at room temperature using X-band frequency.

Structural studies of the glasses by Raman spectroscopy using three different laser sources at 355, 488, and 633 nm confirmed the expected silicate structure of a mixture of Q^3 and Q^2 units for CBS72, with increasing depolymerization to mainly Q^2 units in CBS81. Despite the high hygroscopicity of the samples, no significant water bands or Si–OH bands were visible in the Raman spectra during the time of measurement. The metasilicate glass CBS81 shows next to the majority Q^2 species, also traces of Q^3 and Q^1 due to the disproportionation of $2Q^2 \Longleftrightarrow Q^1+Q^3$. Resonance Raman enhancement was observed for the symmetric stretching modes of tetrahedral MnO_4^{3-} and MnO_4^{2-} anions, ν_1 ($Mn^{5+/6+}$-O), as manifested by the strong and very sharp band at 797 cm^{-1} and a shoulder/broadening toward higher frequencies (ca. 802 cm^{-1}). This band was especially pronounced in Raman measurements using the 488 and 633 nm laser lines; it becomes the dominant Raman feature even at MnO_2 levels as low as 0.5 mol%, and also enables the detection of tetrahedral manganese-oxygen species at doping levels as low as 0.05 mol%.

CRediT authorship contribution statement

Amir Ashjari: Writing – review & editing, Writing – original draft, Visualization, Validation, Investigation, Formal analysis. **Brian Topper:** Writing – review & editing, Writing – original draft, Visualization, Validation, Resources, Investigation, Formal analysis. **Lars H. Hess:** Writing – original draft, Visualization, Investigation, Formal analysis. **Lucas Greiner:** Writing – review & editing, Writing – original draft, Investigation. **Jared Tolliver:** Investigation. **Fiona Cormack:** Investigation. **Dimitrios Palles:** Investigation. **Efstratios I. Kamitsos:** Writing – review & editing, Investigation. **Mikhail G. Brik:** Writing – review & editing, Writing – original draft, Investigation, Formal analysis. **Doris Möncke:** Writing – review & editing, Writing – original draft, Visualization, Supervision, Resources, Project administration, Methodology, Investigation, Formal analysis, Conceptualization.

Declaration of competing interest

The authors declare that they have no known competing financial interests or personal relationships that could have appeared to influence the work reported in this paper.

Data availability

Data will be made available on request.

Acknowledgments

Part of this study (Raman data) is based upon work supported by the National Science Foundation under Grant No. DMR-1626164. We thank B. Rambach, Friedrich Schiller University Jena, for EPR measurements, Lothar Wondraczek, Friedrich Schiller University Jena for helpful discussions and for letting LH pursue unusual oxidation states in his senior thesis. We thank Lenorah Stott and Zainabu Jalango – both from Alfred University (AU) - for their help in melting more glasses, as well as Dominique de Ligny and his group, Friedrich Alexander University Erlangen for remelting a glass for spectroscopic measurements in Athens, Greece. We thank Doris Ehrt, Jena, Germany for heloful discussuin and optical spectra of Mn^{7+}. We also thank Jiao Li and Yiquan Wu for facilitating the supplementary photoluminescence measurements at AU.

MGB thanks the support from the Specialized Funding Program for the Gathering of 100 Elite Talents in Chongqing and the Overseas Talents Plan (Grant No. 2022 [60]) both offered by Chongqing Association for Science and Technology, the Polish NCN projects 2021/40/Q/ST5/00336, the Estonian Research Council grant (PRG 2031), and the Ministry of Science, Technological Development, and Innovation of the Republic of Serbia under contract 451-03-47/2023–01/200017.

Appendix A. Supplementary data

Supplementary data to this article can be found online at https://doi.org/10.1016/j.omx.2024.100371.

References

[1] J.A. Duffy, Bonding, Energy Levels & Bands in Inorganic Solids, Longman Group UK Ltd, 1990.
[2] C.R. Bamford, Colour Generation and Control in Glass, Elsevier Scientific Publishing Company, 1977.
[3] D. Möncke, M. Papageorgiou, A. Winterstein-Beckmann, N. Zacharias, Roman glasses coloured by dissolved transition metal ions: redox-reactions, optical spectroscopy and ligand field theory, J. Archaeol. Sci. 46 (2014) 23–36, https://doi.org/10.1016/j.jas.2014.03.007.
[4] J. Wong, C.A. Angell, Glass Structure by Spectroscopy, Marcel Dekker, Inc., New York, 1976.
[5] J. Ferguson, Spectroscopy of 3d complexes, 159–293, https://doi.org/10.1002/9780470166130.ch3, 1970.
[6] T. Bates, J.D. Mackenzie, Ligand field theory and absorption spectra of transition-metal ions in glasses, in: Modern Aspects of the Vitreous State, Butterworths, London, 1962, pp. 195–254.
[7] D. de Ligny, D. Möncke, Colors in glasses, in: Springer Handbook of Glass, Springer, Cham, 2019, pp. 297–341, https://doi.org/10.1007/978-3-319-93728-1_9.
[8] D. Ehrt, M. Leister, A. Matthai, C. Rüssel, F. Breitbarth, Determination of the redox states of vanadium glasses and melts by different methods, in: Fundamentals in Glass Science and Technology, Vaxjö, Sweden, 1997, pp. 204–211.
[9] M. Leister, D. Ehrt, Chromium redox states in different silicate melts at high temperatures (1400-2000°C), in: 5th ESG, 1999, pp. 40–49. Prague, Czech Republic.
[10] M. Leister, D. Ehrt, G. von der Gönna, C. Russel, F.W. Breitbarth, Redox states and coordination of vanadium in sodium silicates melted at high temperatures, Phys. Chem. Glasses 40 (1999) 319–325.
[11] M. Leister, D. Ehrt, Redox behavior of iron and vanadium ions in silicate melts at temperatures up to 2000 degrees C, Glass, Sci. Technol. 72 (1999) 153–160.
[12] M. Gitter, W. Vogel, Zur Farbe und Struktur ionengefärbter Gläser, Silikattechnik 9 (1978) 36–41.
[13] M. Hunault, J.-L. Robert, M. Newville, L. Galoisy, G. Calas, Spectroscopic properties of five-coordinated Co^{2+} in phosphates, Spectrochimica Acta Part A: Molecular and Biomolecular Spectroscopy 117 (2014) 406–412, https://doi.org/10.1016/j.saa.2013.08.021.
[14] M.D. Ingram, J.A. Duffy, Octahedral–tetrahedral transitions of cobalt(II) in sulphate–chloride glasses, J. Chem. Soc. A (1968) 2575–2578, https://doi.org/10.1039/J19680002575.

[15] D. Möncke, D. Ehrt, Radiation-induced defects in CoO- and NiO-doped fluoride, phosphate, silicate and borosilicate glasses,, Glass Sci. Technol. 75 (2002) 243–253.

[16] L. Galoisy, G. Calas, Role of alkali field strength on the speciation of Ni^{2+} in alkali borate glasses: comparison with crystalline Ni-borates, J. Non-Cryst. Solids 577 (2022) 121320, https://doi.org/10.1016/j.jnoncrysol.2021.121320.

[17] M. Tang, E. Song, Q. Zhang, Selective site occupancy engineering enabling Mn^{5+} activated highly efficient near infrared-II emission in Ba_3BPO_7:Mn^{5+}, Appl. Phys. Lett. 124 (2024) https://doi.org/10.1063/5.0190321.

[18] L.D. Merkle, A. Pinto, H.R. Verdún, B. McIntosh, Laser action from Mn^{5+} in $Ba_3(VO_4)_2$, Appl. Phys. Lett. 61 (1992) 2386–2388, https://doi.org/10.1063/1.108172.

[19] U. Oetliker, M. Herren, H.U. Güdel, U. Kesper, C. Albrecht, D. Reinen, Luminescence properties of Mn^{5+} in a variety of host lattices: effects of chemical and structural variation, J. Chem. Phys. 100 (1994) 8656–8665, https://doi.org/10.1063/1.466720.

[20] J.A. Capobianco, G. Cormier, M. Bettinelli, R. Moncorgé, H. Manaa, Near-infrared intraconfigurational luminescence spectroscopy of the Mn^{5+} ($3d^2$) ion in Ca_2PO_4Cl, $Sr_5(PO_4)_3Cl$, Ca_2VO_4Cl and Sr_2VO_4Cl, J. Lumin. 54 (1992) 1–11, https://doi.org/10.1016/0022-2313(92)90043-9.

[21] J.A. Capobianco, G. Cormier, C.A. Morrison, R. Moncorgé, Crystal-field analyis of Mn^{5+} ($3d^2$) in $Sr_5(PO_4)_3Cl$, Opt. Mater. 1 (1992) 209–216, https://doi.org/10.1016/0925-3467(92)90029-M.

[22] M.F. Hazenkamp, H.U. Güdel, S. Kück, G. Huber, W. Rauw, D. Reinen, Excited state absorption and laser potential of Mn^{5+}-doped $LiMn_3PO_4$, Chem. Phys. Lett. 265 (1997) 264–270, https://doi.org/10.1016/S0009-2614(96)01434-0.

[23] S. Kück, K.L. Schepler, B.H.T. Chai, Evaluation of Mn^{5+}-doped $Sr_5(VO_4)_3F$ as a laser material based on excited-state absorption and stimulated-emission measurements, J. Opt. Soc. Am. B 14 (1997) 957, https://doi.org/10.1364/josab.14.000957.

[24] L.D. Merkle, B.H.T. Chai, Y. Guyot, Spectroscopy of the laser ion Mn^{5+} in $Sr_5(VO_4)_3F$, MRS Proceedings 329 (1993) 239, https://doi.org/10.1557/PROC-329-239.

[25] R. Cao, J. Qiu, X. Yu, X. Sun, Spectroscopic investigation on $BaSO_4$:(Mn^{6+}, Mn^{5+}) crystal, ECS J. Solid State Sci. Tech. 2 (2013) R237–R240, https://doi.org/10.1149/2.020311jss.

[26] E.A. Medina, J. Li, J.K. Stalick, M.A. Subramanian, Intense turquoise colors of apatite-type compounds with Mn^{5+} in tetrahedral coordination, Solid State Sci. 52 (2016) 97–105, https://doi.org/10.1016/j.solidstatesciences.2015.12.001.

[27] X. Zhang, Y. Li, Z. Hu, Z. Chen, J. Qiu, A general strategy for controllable synthesis of $Ba_3(MO_4)_2$:Mn^{5+} (M = V, P) nanoparticles, RSC Adv. 7 (2017) 10564–10569, https://doi.org/10.1039/c6ra28225c.

[28] A. Zandonà, V. Castaing, A.I. Shames, G. Helsch, J. Deubener, A.I. Becerro, M. Allix, A. Goldstein, Oxidation and coordination states assumed by transition metal dopants in an invert ultrabasic silicate glass, J. Non-Cryst. Solids 603 (2023) 122094, https://doi.org/10.1016/j.jnoncrysol.2022.122094.

[29] N. Capobianco, M.O.J.Y. Hunault, C. Loisel, B. Trichereau, F. Bauchau, N. Trcera, L. Galoisy, G. Calas, The representation of skin colour in medieval stained glasses: the role of manganese, J. Archaeol. Sci.: Reports 38 (2021) 103082, https://doi.org/10.1016/j.jasrep.2021.103082.

[30] J.A. Duffy, M.D. Ingram, Optical basicity—V a correlation between the Lewis (optical) basicity of oxyanions and the strengths of Brønsted acids in aqueous solution, J. Inorg. Nucl. Chem. 38 (1976) 1831–1833, https://doi.org/10.1016/0022-1902(76)80098-X.

[31] J.A. Duffy, M.D. Ingram, An interpretation of glass chemistry in terms of the optical basicity concept, J. Non-Cryst. Solids 21 (1976) 373–410, https://doi.org/10.1016/0022-3093(76)90027-2.

[32] J.A. Duffy, A review of optical basicity and its applications to oxidic systems, Geochem. Cosmochim. Acta 57 (1993) 3961–3970, https://doi.org/10.1016/0016-7037(93)90346-X.

[33] R. Moretti, Polymerisation, basicity, oxidation state and their role in ionic modelling of silicate melts, Ann. Geophys. 48 (2005) 583–608.

[34] J.A. Duffy, M.D. Ingram, S. Fong, Effect of basicity on chemical bonding of metal ions in glass and its relevance to their stability, Phys. Chem. Chem. Phys. 2 (2000) 1829–1833, https://doi.org/10.1039/b000489h.

[35] J.A. Duffy, Redox equilibria in glass, J. Non-Cryst. Solids 196 (1996) 45–50, https://doi.org/10.1016/0022-3093(95)00560-9.

[36] Y. Suzuki, S. Kawasaki, M. Ookawa, T. Yokokawa, Basicity of alkaline earth silicate melts based on the Cr^{6+}/Cr^{3+} redox equilibria, Mater. Trans., JIM 36 (1995) 1483–1486, https://doi.org/10.2320/matertrans1989.36.1483.

[37] D. Ehrt, M. Leister, A. Matthai, Redox behaviour in glass forming melts, Molten Salt Forum 5–6 (1998) 547–554.

[38] O. Pinet, I. Hugon, S. Mure, Redox control of nuclear glass, Procedia Materials Sci. 7 (2014) 124–130, https://doi.org/10.1016/j.mspro.2014.10.017.

[39] D. Ehrt, M. Leister, A. Matthai, Polyvalent elements iron, tin and titanium in silicate, phosphate and fluoride glasses and melts, Phys. Chem. Glasses 42 (2001) 231–239.

[40] M. Leister, D. Ehrt, The influence of high melting temperatures on the behaviour of polyvalent ions in silicate glasses, Glass Sci. Technol.: Glastechnische Ber. 73 (2000) 194–203, https://doi.org/10.13140/RG.2.1.3827.9765.

[41] A. Zandonà, V. Castaing, A.I. Shames, G. Helsch, A. Pirri, G. Toci, J. Deubener, M. Allix, A. Goldstein, Effect of the interaction between basicity and reductive character of melting atmosphere – both extreme – on the oxidation and coordination states assumed by transition metals when doped to silicate glasses, J. Non-Cryst. Solids 637 (2024), https://doi.org/10.1016/j.jnoncrysol.2024.123038.

[42] A. Dietzel, M. Coenen, Über dreiwertiges Kobalt in Gläsern hohen Alkaligehaltes, Glastechnische Ber. 34 (1961) 49–56.

[43] L. Heß, Unusual High Oxidation States of d-Transition Metal Ions in Glasses, Friedrich Schiller University, Jena, Germany, 2015. Bachelor Thesis (in German).

[44] M.G. Brik, A.M. Srivastava, On the optical properties of the Mn^{4+} ion in solids, J. Lumin. 133 (2013) 69–72, https://doi.org/10.1016/j.jlumin.2011.08.047.

[45] M.G. Brik, N.M. Avram, C.N. Avram, Exchange charge model of crystal field for 3d ions, in: Optical Properties of 3d-Ions in Crystals: Spectroscopy and Crystal Field Analysis, Springer Berlin Heidelberg, Berlin, Heidelberg, 2013, pp. 29–94, https://doi.org/10.1007/978-3-642-30838-3_2.

[46] M.D. Dramićanin, Ł. Marciniak, S. Kuzman, W. Piotrowski, Z. Ristić, J. Periša, I. Evans, J. Mitrić, V. Đorđević, N. Romčević, M.G. Brik, C.G. Ma, Mn^{5+}-activated $Ca_6Ba(PO_4)_4O$ near-infrared phosphor and its application in luminescence thermometry, Light Sci. Appl. 11 (2022), https://doi.org/10.1038/s41377-022-00958-7.

[47] D. Chen, Y. Zhou, J. Zhong, A review on Mn^{4+} activators in solids for warm white light-emitting diodes, RSC Adv. 6 (2016) 86285–86296, https://doi.org/10.1039/C6RA19584A.

[48] Q. Zhou, L. Dolgov, A.M. Srivastava, L. Zhou, Z. Wang, J. Shi, M.D. Dramićanin, M.G. Brik, M. Wu, Mn^{2+} and Mn^{4+} red phosphors: synthesis, luminescence and applications in WLEDs, A review, J. Mater. Chem. C 6 (2018) 2652–2671, https://doi.org/10.1039/C8TC00251G.

[49] L.D. Merkle, Y. Guyot, B.H.T. Chai, Spectroscopic and laser investigations of Mn^{5+}:$Sr_5(VO_4)_3F$, J. Appl. Phys. 77 (1995) 474–480, https://doi.org/10.1063/1.359585.

[50] H.R. Verdún, Absorption and emission properties of the new laser-active center in Mn^{5+} in several crystalline hosts, in: Advanced Solid State Lasers, OSA, Washington, D.C., 1993, p. TL7, https://doi.org/10.1364/ASSL.1993.TL7.

[51] W.M. Piotrowski, R. Marin, M. Szymczak, E. Martín Rodríguez, D.H. Ortgies, P. Rodríguez-Sevilla, M.D. Dramićanin, D. Jaque, L. Marciniak, Mn^{5+} lifetime-based thermal imaging in the optical transparency windows through skin-mimicking tissue phantom, Adv. Opt. Mater. 11 (2023), https://doi.org/10.1002/adom.202202366.

[52] V. Rajendran, K.-C. Chen, W.-T. Huang, N. Majewska, T. Leśniewski, M. Grzegorczyk, S. Mahlik, G. Leniec, S.M. Kaczmarek, W.K. Pang, V.K. Peterson, K.-M. Lu, H. Chang, R.-S. Liu, Pentavalent manganese luminescence: designing narrow-band near-infrared light-emitting diodes as next-generation compact light sources, ACS Energy Lett. 8 (2023) 289–295, https://doi.org/10.1021/acsenergylett.2c02403.

[53] H. Zhao, X. Xin, Q. Wang, Z. Wang, Y. Wang, Q. Cheng, T. Siritanon, M. A. Subramanian, P. Jiang, Mn^{5+}-doped $BaAl_2O_4$, $Ba_3Al_2O_6$, and $Ba_7Al_2O_{10}$ phosphors emitting in the second near-infrared biological window, J. Alloys Compd. 976 (2024) 173044, https://doi.org/10.1016/j.jallcom.2023.173044.

[54] J.A. Duffy, Optical basicity: a practical acid-base theory for oxides and oxyanions, J. Chem. Educ. 73 (1996) 1138, https://doi.org/10.1021/ed073p1138.

[55] C.P. Rodriguez, J.S. McCloy, M.J. Winschell, A. Schweiger, Optical Basicity and Nepheline Crystallization in High Alumina Glasses, Pacific Northwest National Laboratory, 2011. https://www.pnnl.gov/main/publications/external/technical_reports/PNNL-20184.pdf.

[56] J.A. Duffy, Optical basicity of fluorides and mixed oxide – fluoride glasses and melts, Phys. Chem. Glasses Eur. J. Glass Sci. Technol. B 52(2011)107–114.

[57] L.L. Velli, C.P.E. Varsamis, E.I. Kamitsos, D. Möncke, D. Ehrt, Optical basicity and refractivity in mixed oxyfluoride glasses, Phys. Chem. Glasses Eur. J. Glasses Sci. Technol. B 49 (2008) 182–187.

[58] D. Möncke, S. Ali, B. Jonson, E.I. Kamitsos, Anion polarizabilities in oxynitride glasses. Establishing a common optical basicity scale, Phys. Chem. Chem. Phys. 22 (2020) 9543–9560, https://doi.org/10.1039/C9CP06930E.

[59] V. Dimitrov, T. Komatsu, An interpretation of optical properties of oxides and oxide glasses in terms of the electronic ion polarizability and average single bond strength, J. Univ. Chem. Technol. Metall. 45 (2010) 219–250. https://journal.uctm.edu/node/j2010-3/1_Veselin_Dimitrov_219-250.pdf.

[60] J.A. Duffy, Optical basicity and refractivity of aluminosilicate glasses, Phys. Chem. Glasses 44 (2003) 388–392.

[61] D. Möncke, E.I. Kamitsos, A. Herrmann, D. Ehrt, M. Friedrich, Bonding and ion–ion interactions of Mn^{2+} ions in fluoride-phosphate and boro-silicate glasses probed by EPR and fluorescence spectroscopy, J. Non-Cryst. Solids 357 (2011) 2542–2551, https://doi.org/10.1016/j.jnoncrysol.2011.02.017.

[62] D. Möncke, D. Ehrt, Charge transfer transitions in glasses - attempt of a systematic review, Opt. Mater. X 12 (2021) 100092, https://doi.org/10.1016/j.omx.2021.100092.

[63] M. Brik, C.-G. Ma, Theoretical Spectroscopy of Transition Metal and Rare Earth Ions from Free State to Crystal Field, Jenny Stanford Publishing Pte. Ltd, 2020.

[64] Y. Tanabe, S. Sugano, On the absorption spectra of complex ions II, J. Phys. Soc. Jpn. 9 (1954) 766–779, https://doi.org/10.1143/JPSJ.9.766.

[65] C.R. Bamford, The application of the ligand field theory to coloured glasses, Phys. Chem. Glasses 3 (1962) 189–202.

[66] Y. Tanabe, S. Sugano, On the absorption spectra of complex ions. I, J. Phys. Soc. Jpn. 9 (1954) 753–766, https://doi.org/10.1143/JPSJ.9.753.

[67] M.G. Brik, E. Cavalli, R. Borromei, M. Bettinelli, Crystal field parameters and energy level structure of the MnO_4^{3-} tetroxo anion in Li_3PO_4, Ca_2PO_4Cl and $Sr_5(PO_4)_3Cl$ crystals, J. Lumin. 129 (2009) 801–806, https://doi.org/10.1016/j.jlumin.2009.02.018.

[68] S.K. Gupta, R.M. Kadam, R. Gupta, M. Sahu, V. Natarajan, Evidence for the stabilization of manganese ion as Mn(II) and Mn(IV) in α-$Zn_2P_2O_7$: probed by EPR, luminescence and electrochemical studies, Mater. Chem. Phys. 145 (2014) 162–167, https://doi.org/10.1016/j.matchemphys.2014.01.054.

[69] I. Konidakis, C.-P.E. Varsamis, E.I. Kamitsos, D. Möncke, D. Ehrt, Structure and properties of mixed strontium−manganese metaphosphate glasses, J. Phys. Chem. C 114 (2010) 9125–9138, https://doi.org/10.1021/jp101750t.

[70] D. Möncke, Photo-ionization of 3d-ions in fluoride-phosphate glasses, Int. J. Appl. Glass Sci. 6 (2015) 249–267, https://doi.org/10.1111/ijag.12135.

[71] D. Möncke, D. Ehrt, Irradiation induced defects in glasses resulting in the photoionization of polyvalent dopants, Opt. Mater. 25 (2004) 425–437, https://doi.org/10.1016/j.optmat.2003.11.001.

[72] A. Winterstein-Beckmann, D. Möncke, D. Palles, E.I. Kamitsos, L. Wondraczek, Structure–property correlations in highly modified Sr, Mn-borate glasses, J. Non-Cryst. Solids 376 (2013) 165–174, https://doi.org/10.1016/j.jnoncrysol.2013.05.029.

[73] Z. Liao, H. Xu, W. Zhao, H. Yang, J. Zhong, H. Zhang, Z. Nie, Z.-K. Zhou, Energy transfer from Mn^{4+} to Mn^{5+} and near infrared emission with wide excitation band in $Ca_{14}Zn_6Ga_{10}O_{35}$:Mn phosphors, Chem. Eng. J. 395 (2020) 125060, https://doi.org/10.1016/j.cej.2020.125060.

[74] T.C. Brunold, M.F. Hazenkamp, H.U. Güdel, Luminescence of CrO_4^{3-} and MnO_4^{2-} in various hosts, J. Lumin. 72–74 (1997) 164–165, https://doi.org/10.1016/S0022-2313(96)00179-2.

[75] C. Nelson, W.B. White, Transition metal ions in silicate melts—I. Manganese in sodium silicate melts, Geochem. Cosmochim. Acta 44 (1980) 887–893, https://doi.org/10.1016/0016-7037(80)90269-0.

[76] S. Kück, S. Hartung, S. Hurling, K. Petermann, G. Huber, Emission of octahedrally coordinated Mn^{3+} in garnets, Spectrochimica Acta Part A: Molecular and Biomolecular Spectroscopy 54 (1998) 1741–1749, https://doi.org/10.1016/S1386-1425(98)00106-1.

[77] S. Geschwind, P. Kisliuk, M.P. Klein, J.P. Remeika, D.L. Wood, Sharp-line fluorescence, electron paramagnetic resonance, and thermoluminescence of Mn^{4+} in α-Al_2O_3, Phys. Rev. 126 (1962) 1684–1686, https://doi.org/10.1103/PhysRev.126.1684.

[78] H. Lachwa, D. Reinen, Color and electronic structure of manganese(V) and manganese(VI) in tetrahedral oxo coordination. A spectroscopic investigation, Inorg. Chem. 28 (1989) 1044–1053.

[79] D.L. Griscom, R.E. Griscom, Paramagnetic resonance of Mn^{2+} in glasses and compounds of the lithium borate system, J. Chem. Phys. 47 (1967) 2711–2722, https://doi.org/10.1063/1.1712288.

[80] J. Kliava, EPE of impurity ions in disordered solids distributions of the spin Hamiltonian parameters, Physica Status Solidi (b) 134 (1986) 411–455, https://doi.org/10.1002/pssb.2221340202.

[81] J. Telser, L.A. Pardi, J. Krzystek, L.-C. Brunel, EPR spectra from "EPR-silent" species: high-field EPR spectroscopy of aqueous chromium(II), Inorg. Chem. 37 (1998) 5769–5775, https://doi.org/10.1021/ic9806683.

[82] R. Stoyanova, M. Gorova, E. Zhecheva, EPR of Mn^{4+} in spinels $Li_{1+x}Mn_{2-x}O_4$ with $0 \leq x \leq 0.1$, J. Phys. Chem. Solid. 61 (2000) 609–614, https://doi.org/10.1016/S0022-3697(99)00244-9.

[83] S.K. Misra, L.E. Misiak, J.A. Capobianco, An EPR study of a single crystal of the solid-state-laser material Mn^{5+}-doped $Sr_5(PO_4)_3Cl$, J. Phys. Condens. Matter 6 (1994) 3955–3963, https://doi.org/10.1088/0953-8984/6/21/020.

[84] T. Maksimova, V. Vikhnin, H. Asatryan, K. Hermanowicz, M. Maczka, J. Hanuza, EPR and optical spectroscopy of MnO_4^{2-} doped proper ferroelastic $K_3Na(CrO_4)_2$: local transition and Jahn-Teller effect, Phys. Status Solidi (c) 4 (2007) 843–846, https://doi.org/10.1002/pssc.200673726.

[85] D. Möncke, D. Ehrt, Photoinduced redox reactions in Zr, Nb, Ta, Mo, and W doped glasses, Phys. Chem. Glasses Eur. J. Glasses Sci. Technol. B 48 (2007) 317–323.

[86] E. Schleitzer-Steinkopf, Mangan Teil C2 - Oxomanganionen, in: Gmelin Handbuch der Chemie, Springer, 1975.

[87] F.R. Duke, The disproportionation of manganate ion. manganese dioxide as heterogeneous catalyst, J. Phys. Chem. 56 (1952) 882–884, https://doi.org/10.1021/j150499a014.

[88] A. Berg, Iodates — Iodates doubles de bioxyde de manganèse, C. R. Acad. Sci. 128 (1899) 673.

[89] L.K. Noda, M.C.C. Ribeiro, N.S. Gonçalves, A.H. Jubert, O. Sala, Electronic transitions of the manganate(V) ion in aqueous solution: a resonance Raman study, J. Raman Spectrosc. 30 (1999) 697–704, https://doi.org/10.1002/(SICI)1097-4555(199908)30:8<697::AID-JRS435>3.0.CO;2-U.

[90] L. Antonov, Comment on "Learning to read spectra: Teaching decomposition with excel in a scientific writing course,", J. Chem. Educ. 95 (2018) 1679–1681, https://doi.org/10.1021/acs.jchemed.8b00223.

[91] Y. Shen, T. Riedener, K.L. Bray, Effect of pressure on site-symmetry distortions of Mn^{5+} and Cr^{4+} in Y_2SiO_5, Phys. Rev. B 61 (2000) 9277–9286, https://doi.org/10.1103/PhysRevB.61.9277.

[92] M.G. Brik, I. Sildos, M. Berkowski, A. Suchocki, Spectroscopic and crystal field studies of $YAlO_3$ single crystals doped with Mn ions, J. Phys. Condens. Matter 21 (2009) 025404, https://doi.org/10.1088/0953-8984/21/2/025404.

[93] A. Herrmann, D. Ehrt, Time resolved fluorescence measurements on Tb^{3+} and Mn^{2+} doped glasses, Glass Sci. Technol. 78 (2005) 99–105.

[94] U. Hömmerich, H. Eilers, W.M. Yen, H.R. Verdún, The optical center MnO_4^{3-} in Y_2SiO_5:Mn, X (X=Al, Ca)-, Chem. Phys. Lett. 213 (1993) 163–167, https://doi.org/10.1016/0009-2614(93)85435-Q.

[95] D.L. Griscom, Electron spin resonance in glasses, J. Non-Cryst. Solids 40 (1980) 211–272, https://doi.org/10.1016/0022-3093(80)90105-2.

[96] K. Kioka, T. Honma, T. Ishibashi, T. Komatsu, Laser patterning and magnetic properties of perovskite-type $La_{0.7}Sr_{0.3}MnO_3$ crystals on the glass surface, Solid State Commun. 149 (2009) 1795–1798, https://doi.org/10.1016/j.ssc.2009.07.017.

[97] D. Möncke, D. Ehrt, Photoinduced redox-reactions and transmission changes in glasses doped with 4d- and 5d-ions, J. Non-Cryst. Solids 352 (2006) 2631–2636, https://doi.org/10.1016/j.jnoncrysol.2006.03.034.

[98] S.A. Brawer, W.B. White, Raman spectroscopic investigation of the structure of silicate glasses. I. The binary alkali silicates, J. Chem. Phys. 63 (1975) 2421–2432, https://doi.org/10.1063/1.431671.

[99] L.L. Velli, C.P.E. Varsamis, E.I. Kamitsos, D. Möncke, D. Ehrt, Structural investigation of metaphosphate glasses, Phys. Chem. Glasses 46 (2005) 178–181.

[100] L. Grund Bäck, S. Ali, S. Karlsson, D. Möncke, E.I. Kamitsos, B. Jonson, Mixed alkali/alkaline earth-silicate glasses: physical properties and structure by vibrational spectroscopy, Int. J. Appl. Glass Sci. 10 (2019) 349–362, https://doi.org/10.1111/ijag.13101.

[101] B. Topper, L. Greiner, R.E. Youngman, D. Stohr, E.I. Kamitsos, D. Möncke, Effect of modifier cation size on the structure, properties and nickel speciation in BK7 type alkali borosilicate glasses, J. Non-Cryst. Solids X 17 (2023), https://doi.org/10.1016/j.nocx.2023.100161.

[102] C. O'Shaughnessy, G.S. Henderson, H.W. Nesbitt, G.M. Bancroft, D.R. Neuville, The influence of modifier cations on the Raman stretching modes of Q^n species in alkali silicate glasses, J. Am. Ceram. Soc. 103 (2020) 3991–4001, https://doi.org/10.1111/jace.17081.

[103] McMillan, Structural studies of silicate glasses and melts-applications and limitations of Raman spectroscopy, Am. Mineral. 69 (1984) 622–644.

[104] E.I. Kamitsos, J.A. Kapoutsis, H. Jain, C.H. Hsieh, Vibrational study of the role of trivalent ions in sodium trisilicate glass, J. Non-Cryst. Solids 171 (1994) 31–45, https://doi.org/10.1016/0022-3093(94)90030-2.

[105] I. Efthimiopoulos, D. Palles, S. Richter, U. Hoppe, D. Möncke, L. Wondraczek, S. Nolte, E.I. Kamitsos, Femtosecond laser-induced transformations in ultra-low expansion glass: microstructure and local density variations by vibrational spectroscopy, J. Appl. Phys. 123 (2018), https://doi.org/10.1063/1.5030687.

[106] K. Nakamoto, Infrared and Raman Spectra of Inorganic and Coordination Compounds: Part A: Theory and Applications in Inorganic Chemistry, first ed., Wiley, 2008 https://doi.org/10.1002/9780470405840.

[107] A.H. Jubert, E.L. Varetti, Normal and resonance Raman spectra of some manganates, J. Mol. Struct. 79 (1982) 285–288.

[108] F. Gonzalez-Vilchez, W.P. Griffith, Transition-metal tetra-oxo-complexes and their vibrational spectra, J. Chem. Soc. Dalton Trans. (1972) 1416, https://doi.org/10.1039/dt9720001416.

[109] R. Moncorgé, H. Manaa, G. Boulon, Cr^{4+} and Mn^{5+} active centers for new solid state laser materials, Opt. Mater. 4 (1994) 139–151, https://doi.org/10.1002/pssc.200673726.

[110] N. Sawangboon, A. Nizamutdinova, T. Uesbeck, R. Limbach, E. Meechoowas, K. Tapasa, D. Möncke, L. Wondraczek, E.I. Kamitsos, L. van Wüllen, D.S. Brauer, Modification of silicophosphate glass composition, structure, and properties via crucible material and melting conditions, Int. J. Appl. Glass Sci. 11 (2020) 46–57, https://doi.org/10.1111/ijag.13958.

[111] D.C. Lacy, R. Gupta, K.L. Stone, J. Greaves, J.W. Ziller, M.P. Hendrich, A. S. Borovik, Formation, structure, and EPR detection of a high spin Fe^{IV}—oxo species derived from either an Fe^{III}—oxo or Fe^{III}—OH complex, J. Am. Chem. Soc. 132 (2010) 12188–12190, https://doi.org/10.1021/ja1047818.

[112] G.E. Rindone, J.L. Rhoads, The colors of platinum, palladium, and rhodium in simple glasses, J. Am. Ceram. Soc. 39 (1956) 173–180.

[113] J.A. Duffy, W.J.D. Macdonald, Oxidation states and stereochemistries of some platinum group metals in sulphate and bisulphate melts and glasses, Phys. Chem. Glasses 12 (1971) 87–90.

[114] S. Chen, Y. Chen, J. Cheng, Q. Zhou, W. Chen, L. Hu, G. Boulon, (INVITED) Impurities in large scale produced Nd-doped phosphate laser glasses. II. Pt ion and Pt inclusion, Opt. Mater. X 2 (2019) 100032, https://doi.org/10.1016/j.omx.2019.100032.